

1 This paper presents a very interesting work to develop a simple topography-driven and calibration-free
2 runoff generation module. The module works for saturation excess runoff generation mechanism, which
3 prevails in most humid/semi-humid areas and is demonstrated by some experts to operate in some arid
4 areas also. The module was rigorously compared against the corresponding models in HBV and
5 TOPMODEL. The experiments in both data-rich experimental watersheds and MOPEX catchments
6 support the superiority of the new module (called HSC and HSC-MCT). The authors also discuss the deep
7 reason of why type question (why can HSC outperforms calibrated-type module) in the context of
8 ecological evolution theory. The proposed method has a wide implication for hydrological and ecological
9 research.

10 [We thank the Editor's positive comments.](#)

11
12 Some minor comments are listed below for authors' reference:

13 1. P5L125, one or two sentences should add to explain MCT concisely. This term is not a popular one in
14 hydrological literature. No further explanation will hinder the reader's understanding.

15 [More explanation of MCT is added. \(L158-161\)](#)

16
17 2. P8L214, the term of subsurface flow. Quite a few different terms have been used for the flow in soil
18 media. The authors can refer to Markus Weiler and Jeffery MacDonnell (in Encyclopedia of Hydrological
19 Sciences. Edited by M G Anderson.). In my mind, the term subsurface flow could refer to all kinds of flow
20 types occurring in soil media, including soil matrix flow, preferential flow, or others. I understand the
21 authors mean preferential type flow by subsurface flow here.

22 [This sentence is modified \(L247-248\). And we add more interpretation in the discussion. \(L585-590\)](#)

23
24 3. P16L440, 'interestingly' is not suitable here, because HAND by its definition should not depend on
25 elevation.

26 [Changed. \(L477-479\)](#)

27

28

29

30

31 A simple topography-driven and 32 calibration-free runoff generation module

33 Hongkai Gao^{1,2,3,4*}, Christian Birkel^{5,6}, Markus Hrachowitz⁷, Doerthe Tetzlaff⁶, Chris Soulsby⁶, Hubert H. G. Savenije⁷

34

35 ¹ Key Laboratory of Geographic Information Science (Ministry of Education of China), East China Normal University,
36 Shanghai, China.

37 ² School of Geographical Sciences, East China Normal University, Shanghai, China.

38 ³ Julie Ann Wrigley Global Institute of Sustainability, Arizona State University PO Box 875402. Tempe, AZ 85287-5402.

39 ⁴ Northwest Institute of Eco-Environment and Resources, Chinese Academy of Sciences, Lanzhou, China.

40 ⁵ Department of Geography, University of Costa Rica, San José, Costa Rica

41 ⁶ Northern Rivers Institute, University of Aberdeen, Scotland.

42 ⁷ Water Resources Section, Delft University of Technology, Delft, Netherlands.

43

44 *Corresponding to Hongkai Gao (hkgao@geo.ecnu.edu.cn)

45

46 Abstract

47 Reading landscapes and developing calibration-free runoff generation models that adequately reflect land
48 surface heterogeneities remains the focus of much hydrological research. In this study, we report a novel
49 and simple topography-driven runoff generation parameterization – the HAND-based Storage Capacity
50 curve (HSC), that uses a topographic index (HAND, Height Above the Nearest Drainage) to identify
51 hydrological similarity and the extent of saturated areas in catchments. The HSC can be used as a module
52 in any conceptual rainfall-runoff model. Further, coupling the HSC parameterization with the Mass Curve
53 Technique (MCT) to estimate root zone storage capacity (S_{uMax}), we developed a calibration-free runoff
54 generation module HSC-MCT. The runoff generation modules of HBV and TOPMODEL were used for
55 comparison purposes. The performance of these two modules (HSC and HSC-MCT) was first checked
56 against the data-rich Bruntland Burn (BB) catchment in Scotland, which has a long time series of field-
57 mapped saturation area extent. We found that HSC, HBV and TOPMODEL all perform well to reproduce
58 the hydrograph, but the HSC module performs better in reproducing saturated area variation, in terms of

59 correlation coefficient and spatial pattern. The HSC and HSC-MCT modules were subsequently tested for
60 323 MOPEX catchments in the US, with diverse climate, soil, vegetation and geological characteristics. In
61 comparison with HBV and TOPMODEL, the HSC performs better in both calibration and validation,
62 particularly in the catchments with gentle topography, less forest cover and arid climate. Despite having
63 no calibrated parameters, the HSC-MCT module performed comparably well with calibrated modules,
64 highlighting the robustness of the HSC parameterization to describe the spatial distribution of the root
65 zone storage capacity and the efficiency of the MCT method to estimate S_{uMax} . This novel and calibration-
66 free runoff generation module helps to improve the Prediction in Ungauged Basins and has great potential
67 to be generalized at the global scale.

68

69 1 Introduction

70 Determining the volume and timing of runoff generation from rainfall inputs remains a central challenge
71 in rainfall-runoff modelling (Beven, 2012; McDonnell, 2013). Creating a simple, calibration-free, but robust
72 runoff generation module has been, and continues to be, an essential pursuit of hydrological modellers.
73 Although we have made tremendous advances to enhance our ability on Prediction in Ungauged Basins
74 (PUB) (Sivapalan et al., 2003; Blöschl et al., 2013; Hrachowitz et al., 2013), it is not uncommon that models
75 become increasingly complicated in order to capture the details of hydrological processes shown by
76 empirical studies (McDonnell, 2007; Sivapalan, 2009; Yu et al., 2014). More detailed process
77 conceptualization normally demands higher data requirements than our standard climatological and
78 hydrological networks can provide, leading to more calibrated parameters and a probable increase in
79 model uncertainty (Sivapalan, 2009).

80 Hydrological connectivity is a key characteristic of catchment functioning, controlling runoff generation.
81 It is a property emerging at larger scales, describing the temporal dynamics of how spatially
82 heterogeneous storage thresholds in different parts of catchments are exceeded to contribute to storm
83 runoff generation and how they are thus “connected to the stream” (e.g. Zehe and Blöschl, 2004;
84 Bracken and Croke, 2007; Lehmann et al., 2007; Zehe and Sivapalan, 2009; Ali et al., 2013; Blume and
85 van Meerveld, 2015). Connectivity is controlled by a multitude of factors (Ali and Roy, 2010), including
86 but not limited to surface (e.g. Jencso et al., 2009) and subsurface topography (e.g. Tromp-van Meerveld
87 and McDonnell, 2006), soils (including preferential flow networks; e.g. Zehe et al., 2006; Weiler and
88 McDonnell, 2007), land cover (e.g. Imeson and Prinsen, 2004; Jencso and McGlynn, 2011; Emanuel et al.,

89 2014), the wetness state of the system (e.g. [Detty and McGuire, 2010](#); [Penna et al., 2011](#); [McMillan et](#)
90 [al., 2014](#); [Nippgen et al., 2015](#)).

91 In detailed distributed hydrological bottom-up models, connectivity emerges from the interplay of
92 topography, soil type and water table depth. For example, TOPMODEL ([Beven and Kirkby, 1979](#); [Beven](#)
93 [and Freer, 2001](#)) uses topographic wetness index (TWI) to distinguish hydrologic similarity; and SHE
94 ([Abbott et al. 1986](#)) and tRIBS ([Ivanov et al. 2004](#); [Vivoni et al. 2005](#)) use partial differential equations to
95 describe the water movement based on pressure gradients obtained by topography; and the
96 Representative Elementary Watershed (REW) approach divides catchment into a number of REWs to
97 build balance and constitutive equations for hydrological simulation ([Reggiani et al., 1999](#); [Zhang and](#)
98 [Savenije, 2005](#); [Tian et al., 2008](#)). As the relevant model parameters such as local topographic slope and
99 hydraulic conductivity can, in spite of several unresolved issues for example relating to the differences in
100 the observation and modelling scales (e.g. [Beven, 1989](#); [Zehe et al., 2014](#)), be obtained from direct
101 observations, they could *in principle* be applied without calibration.

102 Zooming out to the macro-scale, top-down models, in contrast, are based on emergent functional
103 relationships that integrate system-internal heterogeneity ([Sivapalan, 2005](#)). These functional
104 relationships require parameters that are effective on the modelling scale and that can largely not be
105 directly determined with small-scale field observations (cf. [Beven, 1995](#)), thus traditionally determined
106 by calibration. However, frequently the number of observed variables for model calibration is, if
107 available at all, limited to time series of stream flow. The absence of more variables to constrain models
108 results in such models being ill-posed inverse problems. Equifinality in parameterization and in the
109 choice of parameters then results in considerable model uncertainty (e.g. [Beven, 1993, 2006](#)). To limit
110 this problem and to also allow predictions in the vast majority of ungauged catchments, it is therefore
111 desirable to find ways to directly infer effective model parameters at the modelling scale from readily
112 available data ([Hrachowitz et al., 2013](#)).

113 The component that is central for establishing connectivity in most top-down models is the soil moisture
114 routine. Briefly, it controls the dynamics of water storage and release in the unsaturated root zone and
115 partitions water into evaporative fluxes, groundwater recharge and fast lateral storm flow generating
116 runoff ([Gao et al., 2018a](#); [Shao et al., 2018](#)). The latter of which is critical from the aspect of connectivity.
117 In majority regions, Hortonian overland flow (HOF, i.e. infiltration excess overland flow) is of minor
118 importance([Dunne and Black, 1970](#); [Sklash and Farvolden, 1979](#); [Beven, 2004](#); [Burt and McDonnell,](#)
119 [2015](#)), even in arid regions where often most locally generated HOF is re-infiltrated while flowing on

120 hillslopes (Liu et al., 2012) and never reaches the stream channel network. Thus the term saturation
121 excess flow (SEF) can represent, depending on the model and the area of application, different
122 processes, such as saturation overland flow, preferential flow, flow through shallow, high permeability
123 soil layers or combinations thereof. The interplay between water volumes that are stored and those that
124 are released laterally to the stream via fast, connected flow paths (“connectivity”) is in most top-down
125 models described by functions between water stored in the unsaturated root zone (“soil moisture”) and
126 the areal proportion of heterogeneous, local storage thresholds that are exceeded and thus
127 “connected” (Zhao et al., 1980). In other words, in those parts of a catchment where the storage
128 threshold is exceeded will generate lateral flows, and can alternatively be interpreted as runoff
129 coefficient (e.g. Ponce and Hawkins, 1996; Perrin and Andreassian, 2001; Fenicia et al., 2007; Bergström
130 and Lindström, 2015). Thus the idea goes back to the variable contributing area concept, assuming that
131 only partial areas of a catchment, where soils are saturated and thus storage thresholds are exceeded,
132 contribute to runoff (Hewlett, 1961; Dunne and Black, 1970; Hewlett and Troendle, 1975). Although
133 originally developed for catchments dominated by saturation overland flow, the extension of the
134 concept to subsurface connectivity, posing that surface and subsurface connectivity are “two sides of
135 the same coin” (McDonnell, 2013), proved highly valuable for models such as Xinanjiang (Zhao et al.,
136 1980), HBV (Bergström and Forsman, 1973; Bergström and Lindström, 2015), SCS-CN (Ponce and
137 Hawkins, 1996; Bartlett et al., 2016), FLEX (Fenicia et al., 2008) and GR4J (Perrin and Andreassian et al.,
138 2001).

139 Among these models, connectivity is formulated in a general form as $C_R=f(S_U(t),S_{UMax},\beta)$, where C_R is the
140 runoff coefficient, i.e. the proportion of the catchment generating runoff, $S_U(t)$ is the catchment water
141 content in the unsaturated root zone at any time t , S_{UMax} is a parameter representing the total storage
142 capacity in the unsaturated root zone and β is a shape parameter, representing the spatial distribution
143 of heterogeneous storage capacities in the unsaturated root zone. The parameters of these functions
144 are typically calibrated. In spite of being the core component of soil moisture routines in many top-down
145 models, little effort was previously invested to find ways to determine the parameters at the catchment-
146 scale directly from available data. An important step towards understanding and quantifying
147 connectivity pattern directly based on observations was recently achieved by intensive experimental
148 work in the Tenderfoot Creek catchments in Montana, US. In their work Jencso et al. (2009) were able to
149 show that connectivity of individual hillslopes in their headwater catchments is highly related to their
150 respective upslope accumulated areas. Using this close relationship, Smith et al. (2013) successfully
151 developed a simple top-down model with very limited need for calibration, emphasizing the value of

152 “enforcing field-based limits on model parameters” (Smith et al., 2016). Based on hydrological landscape
153 analysis, FLEX-Topo model (Savenije, 2010) can dramatically reduce the need for calibration (Gharari et
154 al., 2014), and hold considerable potential for spatial model transferability without the need for
155 parameter re-calibration (Gao et al., 2014a; H. Gao et al., 2016). In a recent development, several
156 studies suggest that S_{uMax} can be robustly and directly inferred from long term water balance data, by
157 the Mass Curve Technique (MCT), ~~without the need for further calibration~~ (Gao et al., 2014; de Boer-
158 Euser et al., 2016; Nijzink et al., 2016). The MCT, that is an engineering method for reservoir design, in
159 which the reservoir size is estimated as a function of accumulated inflow and human water demand. The
160 MCT treats the root zone as a reservoir, and estimates catchment-scale S_{uMax} from measurable
161 hydrometeorological data, without the need for further calibration. This leaves shape parameter β as
162 the only free calibration parameter for soil moisture routines of that form. Topography is often the
163 dominant driver of water movement caused by prevailing hydraulic gradients. More crucially,
164 topography usually provides an integrating indicator for hydrological behavior, since topography is
165 usually closely related with other landscape elements, such as soil vegetation climate and even geology
166 (Seibert et al., 2007; Savenije, 2010; Rempe and Dietrich, 2014; Gao et al., 2014b; Maxwell and Condon,
167 2016; Gomes, 2016). The Height Above the Nearest Drainage (HAND; Rennó et al., 2008; Nobre et al.,
168 2011; Gharari et al., 2011), which can be computed from readily available digital elevation models
169 (DEM), could potentially provide first order estimates of groundwater depth , as there is some
170 experimental evidence that with increasing HAND, groundwater depths similarly increase (e.g. Haria and
171 Shand, 2004; Martin et al., 2004; Molenat et al., 2005, 2008; Shand et al., 2005; Condon and Maxwell,
172 2015; Maxwell and Condon, 2016). HAND can be interpreted as a proxy of the hydraulic head and is thus
173 potentially more hydrologically informative than the topographic elevation above sea level (Nobre et al.,
174 2011). Compared with the TWI in TOPMODEL, HAND is an explicit measure of a physical feature linking
175 terrain to water related potential energy for local drainage (Nobre et al., 2011). More interestingly,
176 topographic structure emerges as a powerful force determining rooting depth under a given climate or
177 within a biome (Figure 1), revealed by a global synthesis of 2,200 root observations of >1000 species
178 (Fan et al., 2017). This leads us to think from ecological perspective to use the topographic information
179 as an indicator for root zone spatial distribution without calibrating the β , and coupling it with the MCT
180 method to estimate the S_{uMax} , eventually create a calibration-free runoff generation module.

181 In this study we are therefore going to test the hypotheses that: (1) HAND can be linked to the spatial
182 distribution of storage capacities and therefore can be used to develop a new runoff generation module
183 (HAND-based Storage Capacity curve, i.e. HSC); (2) the distribution of storage capacities determined by

184 HAND contains different information than the topographic wetness index; (3) the HSC together with water
185 balance-based estimates of S_{uMax} (MCT method) allow the formulation of calibration-free
186 parameterizations of soil moisture routines in top-down models directly based on observations. All these
187 hypotheses will be tested firstly in a small data-rich experimental catchment (the Bruntland Burn
188 catchment in Scotland), and then apply the model to a wide range of larger MOPEX catchments (Model
189 Parameter Estimation Experiment).

190 This paper is structured as follows. In the Methods section, we describe two of our proposed modules, i.e.
191 HSC and HSC-MCT, and two benchmark models (HBV, TOPMODEL). This section also includes the
192 description of other modules (i.e. interception, evaporation and routing) in rainfall-runoff modelling, and
193 the methods for model evaluation, calibration and validation. The Dataset section reviews the empirically-
194 based knowledge of the Bruntland Burn catchment in Scotland and the hydrometeorological and
195 topographic datasets of MOPEX catchments in the US for model comparison. The Results section presents
196 the model comparison results. The Discussion section interprets the relation between rainfall-runoff
197 processes and topography, catchment heterogeneity and simple model, and the implications and
198 limitations of our proposed modules. The conclusions are briefly reviewed in the Summary and
199 Conclusions section.

200 2 Methods

201 Based on our perceptual model that saturation excess flow (SEF) is the dominant runoff generation
202 mechanism in most cases, we developed the HAND-based Storage Capacity curve (HSC) module.
203 Subsequently, estimating the parameter of root zone storage capacity (S_{uMax}) by the MCT method without
204 calibration, the HSC-MCT was developed. In order to assess the performance of our proposed modules,
205 two widely-used runoff generation modules, i.e. HBV power function and TOPMODEL module, were set
206 as benchmarks. Other modules, i.e. interception, evaporation and routing, are kept with identical
207 structure and parameterization for the four rainfall-runoff models (HBV, TOPMODEL, HSC, HSC-MCT,
208 whose names are from their runoff generation modules), to independently diagnose the difference among
209 runoff generation modules (Clark et al., 2008; 2010).

210 2.1 Two benchmark modules

211 **HBV power function**

212 The HBV runoff generation module applies an empirical power function to estimate the nonlinear
 213 relationship between the runoff coefficient and soil moisture (Bergström and Forsman, 1973; Bergström
 214 and Lindström, 2015). The function is written as:

$$215 \quad A_s = \left(\frac{S_u}{S_{uMax}} \right)^\beta \quad (1)$$

216 Where A_s (-) represents the contributing area, which equals to the runoff coefficient of a certain rainfall
 217 event; S_u (mm) represents the averaged root zone soil moisture; S_{uMax} (mm) is the averaged root zone
 218 storage capacity of the studied catchment; β (-) is the parameter determining the shape of the power
 219 function. The prior range of β can be from 0.1 to 5. The $S_u - A_s$ has a linear relation while β equals to 1. And
 220 the shape becomes convex while the β is less than 1, and the shape turns to concave while the β is larger
 221 than 1. In most situations, S_{uMax} and β are two free parameters, cannot be directly measured at the
 222 catchment scale, and need to be calibrated based on observed rainfall-runoff data.

223 **TOPMODEL module**

224 The TOPMODEL assumes topographic information captures the runoff generation heterogeneity at
 225 catchment scale, and the TWI is used as an index to identify rainfall-runoff similarity (Beven and Kirkby,
 226 1979; Sivapalan et al., 1997). Areas with similar TWI values are regarded as possessing equal runoff
 227 generation potential. More specifically, the areas with larger TWI values tend to be saturated first and
 228 contribute to SEF; but the areas with lower TWI values need more water to reach saturation and generate
 229 runoff. The equations are written as follow:

$$230 \quad D_i = \bar{D} + S_{uMax} (\bar{I}_{TW} - I_{TW_i}) \quad (2)$$

$$231 \quad \bar{D} = S_{uMax} - S_u \quad (3)$$

$$232 \quad A_s = \sum A_{s_i}; \quad \text{while } D_i < 0 \quad (4)$$

233 Where D_i (mm) is the local storage deficit below saturation at specific location (i); \bar{D} (mm) is the averaged
 234 water deficit of the entire catchment (Equation 2), which equals to $(S_{uMax} - S_u)$, as shown in Equation 3. I_{TW_i}
 235 is the local I_{TW} value. \bar{I}_{TW} is the averaged TWI of the entire catchment. Equation 2 means in a certain soil
 236 moisture deficit condition for the entire catchment (\bar{D}), the soil moisture deficit of a specific location (D_i),
 237 is determined by the catchment topography (I_{TW} and I_{TW_i}), and the root zone storage capacity (S_{uMax}).

238 Therefore, the areas with D_i less than zero are the saturated areas (A_{s_i}), equal to the contributing areas.
239 The integration of the A_{s_i} areas (A_s), as presented in Equation 4, is the runoff contributing area, which
240 equals to the runoff coefficient of that rainfall event.

241 Besides continuous rainfall-runoff calculation, Equations 2-4 also allow us to obtain the contributing area
242 (A_s) from the estimated relative soil moisture (S_u/S_{uMax}), and then map it back to the original TWI map,
243 which makes it possible to test the simulated contributing area by field measurement. It is worth
244 mentioning that the TOPMODEL in this study is a simplified version, and not identical to the original one,
245 which combines the saturated and unsaturated soil components.

246 2.2 HSC module

247 In the HSC module, we assume 1) [primarily saturation excess flow as the dominant runoff generation](#)
248 [mechanism](#)~~SEF is the dominant runoff generation mechanism, while surface overland flow (SOF) and~~
249 [subsurface flow \(SSF\) cannot be distinguished](#); 2) the local root zone storage capacity has a positive and
250 linear relationship with HAND, from which we can derive the spatial distribution of the root zone storage
251 capacity; 3) rainfall firstly feeds local soil moisture deficit, and no runoff can be generated before local soil
252 moisture being saturated.

253 Figure 2 shows the perceptual HSC module, in which we simplified the complicated 3-D topography of a
254 real catchment into a 2-D simplified hillslope. And then derive the distribution of root zone storage
255 capacity, based on topographic analysis and the second assumption as mentioned in the preceding
256 paragraph. Figure 3 shows the approach to derive the S_u - A_s relation, which are detailed as follows.

257 I. **Generate HAND map.** The HAND map, which represents the relative vertical distance to the
258 nearest river channel, can be generated from DEM ([Gharari et al., 2011](#)). The stream initiation
259 threshold area is a crucial parameter, determining the perennial river channel network
260 ([Montgomery and Dietrich, 1989](#); [Hooshyar et al., 2016](#)), and significantly impacting the HAND
261 values. In this study, the start area was chosen as 40ha for the BB catchment to maintain a close
262 correspondence with observed stream network. And for the MOPEX catchments, the stream
263 initiation area threshold is set as 500 grid cells (4.05 km²), which fills in the range of stream
264 initiation thresholds reported by others (e.g. [Colombo et al., 2007](#); [Moussa, 2008, 2009](#)). HAND
265 maps were then calculated from the elevation of each raster cell above nearest grid cell flagged
266 as stream cell following the flow direction ([Gharari et al., 2011](#)).

- 267 II. **Generate normalized HAND distribution curve.** Firstly, sort the HAND values of grid cells in
 268 ascending order. Secondly, the sorted HAND values were evenly divided into n bands (e.g. 20
 269 bands in this study), to make sure each HAND band has similar area. The averaged HAND value of
 270 each band is regarded as the HAND value of that band. Thirdly, normalize the HAND bands, and
 271 then plot the normalized HAND distribution curve (Figure 2b).
- 272 III. **Distribute S_{uMax} to each HAND band (S_{uMax_i}).** As assumed, the normalized storage capacity of each
 273 HAND band (S_{uMax_i}) increases with HAND value (Figure 2c). Based on this assumption, the
 274 unsaturated root zone storage capacity (S_{uMax}) can be distributed to each HAND band as S_{uMax_i}
 275 (Figure 3a). It is worth noting that S_{uMax} needs to be calibrated in the HSC module, but free of
 276 calibration in the HSC-MCT module.
- 277 IV. **Derive the S_u - A_s curve.** With the number of s saturated HAND bands (Figure 3a-c), the soil
 278 moisture (S_u) can be obtained by Equation 5; and saturated area proportion (A_s) can be obtained
 279 by Equation 6.

$$280 \quad S_u = \frac{1}{n} [\sum_{i=1}^s S_{uMax_i} + S_{uMax_s}(n - s)] \quad (5)$$

$$281 \quad A_s = \frac{s}{n} \quad (6)$$

282 Where S_{uMax_s} is the maximum S_{uMax_i} of all the saturated HAND bands. Subsequently, the A_s - S_u
 283 curve can be derived, and shown in Figure 3d.

284 The SEF mechanism assumes that runoff is only generated from saturation areas, therefore the proportion
 285 of saturation area is equal to the runoff coefficient of that rainfall-runoff event. Based on the S_u - A_s curve
 286 in Figure 3d, generated runoff can be calculated from root zone moisture (S_u). The HSC module also allows
 287 us to map out the fluctuation of saturated areas by the simulated catchment average soil moisture. For
 288 each time step, the module can generate the simulated root zone moisture for the entire basin (S_u). Based
 289 on the S_u - A_s relationship (Figure 3d), we can map S_u back to the saturated area proportion (A_s) and then
 290 visualize it in the original HAND map. Based on this conceptual model, we developed the computer
 291 program and created a procedural module. The technical roadmap can be found in Figure 4.

292 2.3 HSC-MCT module

293 The S_{uMax} is an essential parameter in various hydrological models (e.g. HBV, Xinanjiang, GR4J), which
 294 determines the long-term partitioning of rainfall into infiltration and runoff. [Gao et al., 2014a](#) found that
 295 S_{uMax} represents the adaption of ecosystems to local climate. Ecosystems may design their S_{uMax} based on
 296 the precipitation pattern and their water demand. The storage is neither too small to be mortal in dry

297 seasons, nor too large to consume excessive energy and nutrients. Based on this assumption, we can
298 estimate the S_{uMax} without calibration, by the MCT method, from climatological and vegetation
299 information. More specifically, the average annual plant water demand in the dry season (S_R) is
300 determined by the water balance and the vegetation phenology, i.e. precipitation, runoff and seasonal
301 NDVI. Subsequently, based on the annual S_R , the Gumbel distribution (Gumbel, 1935), frequently used for
302 estimating hydrological extremes, was used to standardize the frequency of drought occurrence. S_{R20y} , i.e.
303 the root zone storage capacity required to overcome a drought once in 20 years, is used as the proxy for
304 S_{uMax} due to the assumption of a “cost” minimization strategy of plants as we mentioned above (Milly,
305 1994), and the fact that S_{R20y} has the best fit with S_{uMax} . The S_{R20y} of the MOPEX catchments can be found
306 in the map of (Gao et al., 2014a).

307 Eventually, with the MCT approach to estimate S_{uMax} and the HSC curve to represent the root zone storage
308 capacity spatial distribution, the HSC-MCT runoff generation module is created, without free parameters.
309 It is worth noting that both the HSC-MCT and HSC modules are based on the HAND derived S_u - A_s relation,
310 and their distinction lays in the methods to obtain S_{uMax} . So far, the HBV power function module has 2 free
311 parameters (S_{uMax} , β). While the TOPMODEL and the HSC both have one free parameter (S_{uMax}). Ultimately
312 the HSC-MCT has no free parameter.

313 2.4 Interception, evaporation and routing modules

314 Except for the runoff generation module in the root zone reservoir (S_{UR}), we need to consider other
315 processes, including interception (S_{IR}) before the S_{UR} module, evaporation from the S_{UR} and the response
316 routine (S_{FR} and S_{SR}) after runoff generation from S_{UR} (Figure 5). Precipitation is firstly intercepted by
317 vegetation canopies. In this study, the interception was estimated by a threshold parameter (S_{iMax}), set to
318 2 mm (Gao et al., 2014a), below which all precipitation will be intercepted and evaporated (Equation 9)
319 (de Groen and Savenije, 2006). For the S_{UR} reservoir, we can either use the HBV beta-function (Equation
320 12), the runoff generation module of TOPMODEL (Equation 2-4) or the HSC module (Section 2.3) to
321 partition precipitation into generated runoff (R_u) and infiltration. The actual evaporation (E_a) from the soil
322 equals to the potential evaporation (E_p), if S_u/S_{uMax} is above a threshold (C_e), where S_u is the soil moisture
323 and S_{uMax} is the catchment averaged storage capacity. And E_a linearly reduces with S_u/S_{uMax} , while S_u/S_{uMax}
324 is below C_e (Equation 13). The E_p can be calculated by the Hargreaves equation (Hargreaves and Samani,
325 1985), with maximum and minimum daily temperature as input. The generated runoff (R_u) is further split
326 into two fluxes, including the flux to the fast response reservoir (R_f) and the flux to the slow response
327 reservoir (R_s), by a splitter (D) (Equation 14, 15). The delayed time from rainfall peak to the flood peak is

328 estimated by a convolution delay function, with a delay time of T_{lagf} . Subsequently, the fluxes into two
 329 different response reservoirs (S_{FR} and S_{SR}) were released by two linear equations between discharge and
 330 storage (Equation 19, 21), representing the fast response flow and the slow response flow mainly from
 331 groundwater reservoir. The two discharges (Q_f and Q_s) generated the simulated streamflow (Q_m). The
 332 model parameters are shown in Table 1, while the equations are given in Table 2. More detailed
 333 description of the model structure can be referred to [Gao et al., 2014b and 2016](#). It is worth underlining
 334 that the only difference among the benchmark HBV type, TOPMODEL type, HSC, and HSC-MCT models is
 335 their runoff generation modules. Eventually, there are 7 free parameters in HBV model, 6 in TOPMODEL
 336 and HSC model, and 5 in the HSC-MCT model.

337 2.5 Model evaluation, calibration, validation and models comparison

338 Two objective functions were used to evaluate model performance, since multi-objective evaluation is a
 339 more robust approach to quantifying model performance with different criteria than a single one. The
 340 Kling-Gupta efficiency ([Gupta et al., 2009](#)) (I_{KGE}) was used as the criteria to evaluate model performance
 341 and as an objective function for calibration. The equation is written as:

$$342 \quad I_{KGE} = 1 - \sqrt{(r-1)^2 + (\alpha-1)^2 + (\varepsilon-1)^2} \quad (7)$$

343 Where r is the linear correlation coefficient between simulation and observation; α ($\alpha = \sigma_m / \sigma_o$) is a
 344 measure of relative variability in the simulated and observed values, where σ_m is the standard deviation
 345 of simulated streamflow, and σ_o is the standard deviation of observed streamflow; ε is the ratio between
 346 the average value of simulated and observed data. And the I_{KGL} (I_{KGE} of the logarithmic flows) ([Fenicia et](#)
 347 [al., 2007; Gao et al., 2014b](#)) is used to evaluate the model performance on baseflow simulation.

348 A multi-objective parameter optimization algorithm (MOSCEM-UA) ([Vrugt et al., 2003](#)) was applied for
 349 the calibration. The parameter sets on the Pareto-frontier of the multi-objective optimization were
 350 assumed to be the behavioral parameter sets and can equally represent model performance. The
 351 averaged hydrograph obtained by all the behavioral parameter sets were regarded as the simulated result
 352 of that catchment for further studies. The number of complexes in MOSCEM-UA were set as the number
 353 of parameters (7 for HBV, 6 for TOPMODEL and the HSC model, and 5 for HSC-MCT model), and the
 354 number of initial samples was set to 210 and a total number of 50000 model iterations for all the
 355 catchment runs. For each catchment, the first half period of data was used for calibration, and the other
 356 half was used to do validation.

357 In module comparison, we defined three categories: if the difference of I_{KGE} of model A and model B in
358 validation is less than 0.1, model A and B are regarded as “equally well”. If the I_{KGE} of model A is larger
359 than model B in validation by 0.1 or more, model A is regarded as outperforming model B. If the I_{KGE} of
360 model A is less than model B in validation by -0.1 or less, model B is regarded as outperforming model A.

361 3 Dataset

362 3.1 The Bruntland Burn catchment

363 The 3.2 km² Bruntland Burn catchment (Figure 6), located in north-eastern Scotland, was used as a
364 benchmark study to test the ~~models~~model’s performance based on a rich data base of hydrological
365 measurements. The Bruntland Burn is a typical upland catchment in North West Europe (e.g. [Birkel et al.,](#)
366 [2010](#)), namely a combination of steep and rolling hillslopes and over-widened valley bottoms due to the
367 glacial legacy of this region. The valley bottom areas are covered by deep (in parts > 30m) glacial drift
368 deposits (e.g. till) containing a large amount of stored water superimposed on a relatively impermeable
369 granitic solid geology ([Soulsby et al., 2016](#)). Peat soils developed (> 1m deep) in these valley bottom areas,
370 which remain saturated throughout most of the year with a dominant near-surface runoff generation
371 mechanism delivering runoff quickly via micro-topographical flow pathways connected to the stream
372 network ([Soulsby et al., 2015](#)). Brown rankers, peaty rankers and peat soils are responsible for a flashy
373 hydrological regime driven by saturation excess overland flow, while humus iron podzols on the hillslopes
374 do not favor near-surface saturation but rather facilitate groundwater recharge through vertical water
375 movement ([Tetzlaff et al., 2014](#)). Land-use is dominated by heather moorland, with smaller areas of rough
376 grazing and forestry on the lower hillslopes. Its annual precipitation is 1059 mm, with the summer months
377 (May-August) generally being the driest ([Ali et al., 2013](#)). Snow makes up less than 10% of annual
378 precipitation and melts rapidly below 500m. The evapotranspiration is around 400 mm per year and
379 annual discharge around 659 mm. The daily precipitation, potential evaporation, and discharge data range
380 from January 1 in 2008 to September 30 in 2014. The calibration period is from January 1, 2008 to
381 December 31, 2010, and the data from January 1, 2011 to September 30, 2014 is used as validation.

382 The LiDAR-derived DEM map with 2m resolution shows elevation ranging from 250m to 539m (Figure 6).
383 There are 7 saturation area maps (Figure 7) (May 2, July 2, August 4, September 3, October 1, November
384 26, in 2008, and January 21, in 2009), measured directly by the “squishy boot” method and field mapping
385 by global positioning system (GPS), to delineate the boundary of saturation areas connected to the stream
386 network ([Birkel et al., 2010](#); [Ali et al., 2013](#)). These saturation area maps revealed a dynamic behavior of

387 expanding and contracting areas connected to the stream network that were used as a benchmark test
388 for the HSC module.

389 3.2 MOPEX catchments

390 The MOPEX dataset was collected for a hydrological model parameter estimation experiment (Duan et al.,
391 2006; Schaake et al., 2006), containing 438 catchments in the CONUS (Contiguous United States). The
392 longest time series range from 1948 to 2003. 323 catchments were used in this study (see the name list
393 in SI), with areas between 67 and 10,329 km², and excluding the catchments with data records <30 years,
394 impacted by snowmelt or with extreme arid climate (aridity index $E_p/P > 2$). In order to analyze the impacts
395 of catchment characteristics on model performance, excluding hydrometeorology data, we also collected
396 the datasets of topography, depth to rock, soil texture, land use, and stream density (Table 3). These
397 characteristics help us to understand in which catchments the HSC performs better or worse than the
398 benchmark models.

399 **Hydrometeorology**

400 The dataset contains the daily precipitation, daily maximum and minimum air temperature, and daily
401 streamflow. The daily streamflow was used to calibrate the free ~~parameters, and~~ parameters and validate
402 the models.

403 **Topography**

404 The Digital Elevation Model (DEM) of the CONUS in 90m resolution was download from the Earth Explorer
405 of United States Geological Survey (USGS, <http://earthexplorer.usgs.gov/>). The HAND and TWI map can
406 be generated from DEM. The averaged elevation and HAND are used to as two catchment characteristics.

407 **Soil texture**

408 In this study, soil texture is synthetically represented by the K factor, since the K factor is a lumped soil
409 erodibility factor which represents the soil profile reaction to soil detachment (Renard et al., 2011).
410 Generally, the soils (high in clay and sand) have low K values, and soils with high silt content have larger K
411 values. The averaged K factor for each catchment was calculated from soil survey information available
412 from USGS (Wolock, 1997).

413 **Land use**

414 Land use data was obtained from National Land Cover Database (NLCD, <http://www.mrlc.gov/nlcd.php>).
415 Forest plays an essential role in hydrological processes (Gao et al., 2018a), especially for the runoff
416 generation (Brooks et al., 2010). Forest area proportion was utilized as an integrated indicator to represent
417 the impact of vegetation cover on hydrological processes.

418 **Stream density**

419 Stream density (km/km^2) is the total length of all the streams and rivers in a drainage basin divided by the
420 total area of the drainage basin. Stream density data was obtained from Horizon Systems Corporation
421 (<http://www.horizon-systems.com/nhdplus/>).

422 **Geology**

423 Bedrock is a relative impermeable layer, as the lower boundary of subsurface stormflow in the catchments
424 where soil depth is shallow (Tromp-van Meerveld & McDonnell). The depth to bedrock, as an integrated
425 geologic indicator, was accessed from STATSGO (State Soil Geographic,
426 http://www.soilinfo.psu.edu/index.cgi?soil_data&conus&data_cov&dtb) (Schwarz & Alexander, 1995).
427 The averaged depth to bedrock for each catchment was calculated for further analysis.

428 **4 Results of the Bruntland Burn**

429 **4.1 Topography analysis**

430 The generated HAND map, derived also from the DEM, is shown in Figure 6, with HAND values ranging
431 from 0m to 234m. Based on the HAND map, we can derive the S_u - A_s curve (Figure 8) by analyzing the
432 HAND map with the method in Section 2.3. The TWI map of the BB (Figure 6) was generated from its DEM.
433 Overall, the TWI map, ranging from -0.4 to 23.4, mainly differentiates the valley bottom areas with the
434 highest TWI values from the steeper slopes. This is probably caused by the fine resolution of the DEM map
435 in 2 m, as previous research found that the sensitivity of TWI to DEM resolution (Sørensen and Seibert,
436 2007). From the TWI map, the frequency distribution function and the accumulative frequency
437 distribution function can be derived (Figure 8), with one unit of TWI as interval.

438 **4.2 Model performance**

439 It is found that all the three models (HBV, TOPMODEL, and HSC) can perform well in reproducing the
440 observed hydrograph (Figure 9). The I_{KGE} of the three models are all around 0.66 in calibration, which is
441 largely in line with other studies from the BB (Birkel et al, 2010; 2014). And the I_{KGL} are 0.76, 0.72 and 0.74
442 for HSC, HBV and TOPMODEL respectively in calibration. While in validation, I_{KGE} of the three models are

443 also around 0.66, while I_{KGL} are 0.75, 0.70 and 0.65 for the three models. Since the measured rainfall-
444 runoff time series only lasts from 2008 to 2014, which is too short to estimate the S_{R20y} (proxy for S_{UMax})
445 by MCT approach (which needs long-term hydro-meteorological observation data,) the HSC-MCT model
446 was not applied to this catchment.

447 Figure 8 shows the calibrated power curve by HBV (averaged $\beta=0.98$) with the S_u-A_s curve obtained
448 from the HSC module. We found the two curves are largely comparable, especially while the relative soil
449 moisture is low. This result demonstrates that for the BB catchment with glacial drift deposits and
450 combined terrain of steep and rolling hillslopes and over-widened valley bottoms, the HBV power curve
451 can essentially be derived from the S_u-A_s curve of HSC module merely by topographic information without
452 calibration.

453 The normalized relative soil moisture of the three model simulations are presented in Figure 9. Their
454 temporal fluctuation patterns are comparable. Nevertheless, the simulated soil moisture by TOPMODEL
455 has larger variation, compared with HBV and HSC (Figure 9).

456 4.3 Contributing area simulation

457 The observed saturation area and the simulated contributing area from both TOPMODEL and the HSC are
458 shown in Figure 7, 9, 10. We found although both modules overestimated the saturated areas, they can
459 capture the temporal variation. For example, the smallest saturated area both observed and simulated
460 occurred on July-02-2008, and the largest saturated area both occurred on January-21-2009. Comparing
461 the estimated contributing area of TOPMODEL with the HSC module, we found the results of the HSC
462 correlates better ($R^2=0.60$, $I_{KGE}=-3.0$) with the observed saturated areas than TOPMODEL ($R^2=0.50$, $I_{KGE}=-$
463 3.4) (Figure 10). For spatial patterns, the HSC contributing area is located close to the river ~~network,~~
464 ~~and network and~~ reflects the spatial pattern of observed saturated area. While TOPMODEL results are
465 more scattered, probably due to the sensitivity of TWI to DEM resolution (Figure 7). The HSC is more
466 discriminating in terms of less frequently giving an unrealistic 100% ~~saturation, and saturation and~~
467 retaining unsaturated upper hillslopes.

468 5 Results from the MOPEX catchments

469 5.1 Topography analysis of the Contiguous US and 323 MOPEX catchments

470 To delineate the TWI map for the CONUS, the depressions of the DEM were firstly filled with a threshold
471 height of 100m (recommended by Esri). The TWI map of the CONUS is produced (Figure S1). Based on the

472 TWI map of the CONUS, we clipped the TWI maps for the 323 MOPEX catchments with their catchment
473 boundaries. And then the TWI frequency distribution and the accumulated frequency distribution of the
474 323 MOPEX catchments (Figure S2), with one unit of TWI as interval, were derived based on the 323 TWI
475 maps.

476 In Figure 11, it is shown that the regions with large HAND values are located in Rocky Mountains and
477 Appalachian Mountains, while the Great Plains has smaller HAND values. Interestingly, the Great Basin,
478 especially in the Salt Lake Desert, has small HAND values, illustrating its low elevation above the nearest
479 drainage, ~~although their~~ despite a high elevations above seas level ~~are high~~. From the CONUS HAND map,
480 we clipped the HAND maps for the 323 MOPEX catchments with their catchment boundaries. We then
481 plot their HAND-area curves, following the procedures of I and II in Section 2.2. Figure 12a shows the
482 normalized HAND profiles of the 323 catchments.

483 Based on the HAND profiles and the Step III in Section 2.2, we derived the normalized storage capacity
484 distribution for all catchments (Figure 12b). Subsequently, the root zone moisture and saturated area
485 relationship (A_s-S_u) can be plotted by the method in Step IV of Section 2.2. Lastly, reversing the curve of
486 A_s-S_u to S_u-A_s relation (Figure 12c), the latter one can be implemented to simulate runoff generation by
487 soil moisture. Figure 12c interestingly shows that in some catchments, there is almost no threshold
488 behavior between rainfall and runoff generation, where the catchments are covered by large areas with
489 low HAND values and limited storage capacity. Therefore, when rainfall occurs, wetlands response quickly
490 and generate runoff without a precipitation–discharge threshold relationship characteristic of areas with
491 higher moisture deficits. This is similar to the idea of FLEX-Topo where the storage capacity is distinguished
492 between wetlands and hillslopes, and on wetlands, with low storage capacity, where runoff response to
493 rainfall is almost instantaneous.

494 5.2 Model performance

495 Overall, the performance of the two benchmark models, i.e. HBV and TOPMODEL, for the MOPEX data
496 (Figure 13) is comparable with the previous model comparison experiments, conducted with four rainfall-
497 runoff models and four land surface parameterization schemes (Duan et al., 2006; Kollat et al., 2012; Ye
498 et al., 2014). The median value of I_{KGE} of the HBV type model is 0.61 for calibration in the 323 catchments
499 (Figure 13), and averaged I_{KGE} in calibration is 0.62. In validation, the median and averaged values of I_{KGE}
500 are kept the same as calibration. The comparable performance of models in calibration and validation
501 demonstrates the robustness of benchmark models and the parameter optimization algorithm (i.e.
502 MOSCEM-UA). The TOPMODEL improves the median value of I_{KGE} from 0.61 (HBV) to 0.67 in calibration,

503 and from 0.61 (HBV) to 0.67 in validation. But the averaged values of I_{KGE} for TOPMODEL are slightly
504 decreased from 0.62 (HBV) to 0.61 in both calibration and validation. The HSC module, by involving the
505 HAND topographic information without calibrating the β parameter, improves the median value of I_{KGE} to
506 0.68 for calibration and 0.67 for validation. The averaged values of I_{KGE} in both calibration and validation
507 are also increased to 0.65, comparing with HBV (0.62) and TOPMODEL (0.61). Furthermore, Figure 13
508 demonstrates that, comparing with the benchmark HBV and TOPMODEL, not only the median and
509 averaged values were improved by the HSC module, but also the 25th and 75th percentiles and the lower
510 whisker end, all have been improved. The performance gains on baseflow (I_{KGL}) have been investigated
511 and shown in the supplementary figure S3. These results indicate the HSC module improved model
512 performance to reproduce hydrograph for both peak flow (I_{KGE}) and baseflow (I_{KGL}).

513 Additionally, for HSC-MCT model, the median I_{KGE} value is improved from 0.61 (HBV) to 0.65 in calibration,
514 and from 0.61 (HBV) to 0.64 in validation, but not as well performed as TOPMODEL (0.67 for calibration
515 and validation). For the averaged I_{KGE} values, they were slightly reduced from 0.62 (HBV) and 0.61
516 (TOPMODEL) to 0.59 for calibration and validation. Although the HSC-MCT did not perform as well as the
517 HSC module, considering there is no free parameters to calibrate, the median I_{KGE} value of 0.64 (HBV is
518 0.61) and averaged I_{KGE} of 0.59 (TOPMODEL is 0.61) are quite acceptable. In addition, the 25th and 75th
519 percentiles and the lower whisker end of the HSC-MCT model are all improved compared to the HBV
520 model. Moreover, the largely comparable results between the HSC and the HSC-MCT modules
521 demonstrate the feasibility of the MCT method to obtain the S_{uMax} parameter and the potential for HSC-
522 MCT to be implemented in prediction of ungauged basins.

523 Figure 14 shows the spatial comparisons of the HSC and HSC-MCT models with the two benchmark models.
524 We found that the HSC performs “equally well” as HBV (the difference of I_{KGE} in validation ranges -0.1 ~
525 0.1) in 88% catchments, and in the remaining 12% of the catchments the HSC outperforms HBV (the
526 improvement of I_{KGE} in validation is larger than 0.1). In not a single catchment did the calibrated HBV
527 outperform the HSC. Comparing the HSC model with TOPMODEL, we found in 91% of the catchments that
528 the two models have approximately equal performance. In 8% of the catchments, the HSC model
529 outperformed TOPMODEL. Only in 1% of the catchments (two in the Appalachian Mountains and one in
530 the Rocky Mountains in California), TOPMODEL performed better.

531 In order to further explore the impact of catchment characteristics on model performance, we used
532 topography (averaged HAND, averaged slope, and averaged elevation), soil (K-factor), land cover (forest
533 area proportion), climate (aridity index), stream density, and geology (depth to rock) information to test

534 the impact of catchment features on model performance. Table 4 clearly shows that compared with HBV,
535 the 39 catchments with better performance have lower HAND values (37m), more gentle slopes (4.0
536 degree), and smaller forest area (22%); while the elevation, K-factor, aridity index, stream density and
537 depth to rock are almost similar. Also, in the catchments where HSC outperformed TOPMODEL, the
538 catchments have smaller HAND (27m), more gentle slopes (3.6 degree), moderate elevation (469 m), less
539 forest proportion (14%), and more arid climate (aridity index is 1.3). TOPMODEL performs better in only
540 three catchments with larger HAND (193m), steeper slopes (13.5 degree), higher elevation (740 m), more
541 humid climate (aridity index is 0.8), and larger depth to rock (333 cm). In summary, the HSC showed better
542 performance in catchments with gentle topography and more arid climate.

543 Without calibration of S_{uMax} , as expected, the performance of HSC-MCT module slightly deteriorates
544 (Figure 13). In comparison with HBV, the outperformed percentage reduced from 12% (HSC) to 4% (HSC-
545 MCT), the approximately equal-well simulated catchments dropped from 88% to 79%, and the inferior
546 performance increased from 0% to 17%. Also, in comparison with TOPMODEL, the better performance
547 dropped from 8% (HSC) to 7% (HSC-MCT), the approximately equal catchments reduced from 91% to 72%,
548 and the inferior performance increased from 1% to 21%. The inferiority of the HSC-MCT model is probably
549 caused by the uncertainty of the MCT method for different ecosystems which have different survival
550 strategies and use different return periods to bridge critical drought periods. By using ecosystem
551 dependent return periods, this problem could be reduced (Wang-Erlandsson et al., 2016).

552 To further explore the reason for the better performance of the HSC approach, we selected the 08171000
553 catchment in Texas (Figure 14), in which both the HSC module and the HSC-MCT module outperformed
554 the two benchmark modules to reproduce the observed hydrograph (Figure S4). The HBV model
555 dramatically underestimated the peak flows, with I_{KGE} as 0.54, while TOPMODEL significantly
556 overestimated the peak flows, with I_{KGE} as 0.30. The HSC-MCT model improved the I_{KGE} to 0.71, and the
557 HSC model further enhanced I_{KGE} to 0.74.

558 Since the modules of interception, evaporation and routing are identical for the four models, the runoff
559 generation modules are the key to understand the difference in model performance. Figure S5 shows the
560 HBV β curve and the S_u-A_s curve of the HSC model, as well the TWI frequency distribution. We found that
561 with a given S_u/S_{uMax} , the HBV β function generates less contributing area than the HSC model, which
562 explains the underestimation of the HBV model. In contrast, TOPMODEL has a sharp and steep
563 accumulated TWI frequency curve. In particular, the region with TWI=8 accounts for 40% of the catchment
564 area, and over 95% of the catchment areas are within the TWI ranging from 6 to 12. This indicates that

565 even with low soil moisture content (S_u/S_{uMax}), the contributing area by TOPMODEL is relatively large,
566 leading to the sharply increased peak flows for all rainfall events.

567 6 Discussion

568 6.1 Rainfall-runoff processes and topography

569 We applied a novel approach to derive the relationship between soil moisture storage and the saturated
570 area from HAND. The areas with relatively low HAND values are saturated earlier than areas with higher
571 HAND values, due to the larger storage capacity in higher HAND locations. The outperformance of the HSC
572 over the benchmark HBV and TOPMODEL in gentle sloping catchments indicates that the HSC module
573 likely has a higher realism than the calibrated HBV beta-function and the TWI of TOPMODEL in these
574 regions. Very interestingly, [Fan et al., \(2017\)](#) presented an ecological observation in global scale, and
575 revealed the systematic variation of rooting depth along HAND (Fig.1, in [Fan et al., 2017](#)). Since rooting
576 depth can be translated to root zone storage capacity through combination with soil plant-available water
577 ([Wang-Erlandsson et al., 2016](#)). This large sample dataset, from ecological perspective, provides a strong
578 support for the assumption of the HSC model on gentle slopes, i.e. the increase of root zone storage
579 capacity with HAND. More interestingly, on excessively drained uplands, rooting depth does not follow
580 the same pattern, with shallow depth and limited to rain infiltration (Fig.1, in [Fan et al., 2017](#)). This could
581 explain the inferior performance of HSC model to TOPMODEL in three MOPEX catchments with
582 excessively drained uplands (larger HAND, steeper slope, higher elevation, and deeper depth to rock),
583 where Hortonian overland flow is likely the dominant mechanism, and the HSC assumption likely does not
584 work well. This indicates that comparing with TWI, the HAND is closer to catchment realism distinguishing
585 hydrological similarity in gentle topography catchments. [The HSC module assumes SEF as the dominant
586 mechanism. But since in a real catchment different runoff generating processes may act simultaneously
587 in different environments \(McDonnell, 2013; Hrachowitz and Clark, 2017\). Such SEF dominated
588 catchments, or parts thereof, are typically characterized by a subdued relief and thus gently sloping. In
589 steeper catchments, where the groundwater table is deeper and thus more additional water can be stored
590 in the soil, another conceptual parametrisation would be appropriate.](#)

591 The FLEX-Topo model ([Savenije, 2010](#)) also uses HAND as a topographic index to distinguish between
592 landscape-related runoff ~~processes, and~~ processes and has both similarity and differences with the HSC
593 model. The results of the HSC model illustrate that the riparian areas are more prone to be saturated,
594 which is consistent with the concept of the FLEX-Topo model. Another important similarity of the two

595 models is their parallel model structure. In both models it is assumed that the upslope area has larger
596 storage capacity, therefore the upper land generates runoff less and later than the lower land. In other
597 words, in most cases, the local storage is saturated due to the local rainfall, instead of flow from upslope.
598 The most obvious difference between the HSC and the FLEX-Topo is the approach towards discretization
599 of a catchment. The FLEX-Topo model classifies a catchment into various landscapes, e.g. wetlands,
600 hillslopes and plateau. This discretization method requires threshold values to classify landscapes, i.e.
601 threshold values of HAND and slope, which leads to fixed and time-independent proportions of landscapes.
602 The HSC model does not require landscape classification, which reduced the subjectivity in discretization
603 and restricted the model complexity, as well as simultaneously allowing the fluctuation of contributing
604 areas (termed as wetlands in FLEX-Topo).

605 6.2 Catchment heterogeneity and simple models

606 Catchments exhibit a wide array of heterogeneity and complexity with spatial and temporal variations of
607 landscape characteristics and climate inputs. For example, the Darcy-Richards equation approach is often
608 consistent with point-scale measurements of matrix flow, but not for preferential flow caused by roots,
609 soil fauna and even cracks and fissures (Beven and Germann, 1982; Zehe and Fluehler, 2001; Weiler and
610 McDonnell, 2007). As a result, field experimentalists continue to characterize and catalogue a variety of
611 runoff processes, and hydrological and land surface modelers are developing more and more complicated
612 models to involve the increasingly detailed processes (McDonnell et al., 2007). However, there is still no
613 compelling evidence to support the outperformance of sophisticated “physically-based” models in terms
614 of higher equifinality and uncertainty than the simple lumped or semi-distributed conceptual models in
615 rainfall-runoff simulation (Beven, 1989; Orth et al., 2015).

616 But evidence is mounting that a catchment is not a random assemblage of different heterogeneous parts
617 (Sivapalan, 2009; Troch et al., 2013; Zehe et al., 2013), and conceptualising heterogeneities does not
618 require complex laws (Chase, 1992; Passalacqua et al., 2015). Parsimonious models (e.g. Perrin et al.,
619 2003), with empirical curve shapes, likely result in good model performance. Parameter identifiability in
620 calibration is one of the reasons. However, the physical rationale of these parsimonious models is still
621 largely unknown lacking a physical explanation to interpret these empirical curves described by
622 mathematical functions (e.g. Equation 3 in Perrin et al., 2003).

623 The benefits of the new HSC module are two-fold. From a technical point of view, the HSC allows us to
624 make Prediction in Ungauged Basins without calibrating the beta parameter in many conceptual
625 hydrological models. Furthermore, the HSC module, from a scientific point of view, provides us with a new

626 perspective on the linkage between the spatial distribution patterns of root zone storage capacity (long-
627 term ecosystem evolution) with associated runoff generation (event scale rainfall-runoff generation).

628 Asking questions of “why” rather than “what” likely leads to more useful insights and a new way forward
629 (McDonnell et al., 2007). The HSC module provides us with a rationale from an ecological perspective to
630 understand the linkage and mechanism between large-sample hillslope ecological observations and the curve
631 of root zone storage capacity distribution (Figure 1, 2, 3). Catchment is a geomorphological and even an
632 ecological system whose parts are related to each other probably due to catchment self-organization and
633 evolution (Sivapalan and Blöschl, 2015; Savenije and Hrachowitz, 2017). This encourages the hope that
634 simplified concepts may be found adequate to describe and model the operation of the basin runoff
635 generation process. It is clear that topography, with fractal characteristic (Rodriguez-Iturbe and Rinaldo,
636 1997), is often the dominant driver of runoff, as well as being a good integrated indicator for vegetation
637 cover (Gao et al., 2014b), rooting depth (Fan et al., 2017), root zone evaporation and transpiration deficits
638 (Maxwell and Condon, 2016), soil properties (Seibert et al., 2007), and even geology (Rempe and Dietrich,
639 2014; Gomes, 2016). Therefore, we argue that increasingly detailed topographic information is an
640 excellent integrated indicator allowing modelers to continue systematically represent heterogeneities and
641 simultaneously reduce model complexity. The model structure and parameterization of both HSC and
642 TOPMODEL are simple, but not over simplified, as they capture likely the most dominant factor controlling
643 runoff generation, i.e. the spatial heterogeneity of storage capacity. Hence, this study also sheds light on
644 the possibility of moving beyond heterogeneity and process complexity (McDonnell et al., 2007), to
645 simplify them into a succinct and *a priori* curve by taking advantage of catchment self-organization
646 probably caused by co-evolution or the principle of maximum entropy production (Kleidon and Lorenz,
647 2004).

648 6.3 Implications and limitation

649 The calibration-free HSC-MCT runoff generation module enhances our ability to predict runoff in
650 ungauged basins. PUB is probably not a major issue in the developed world, with abundant of
651 comprehensive measurements in many places, but for the developing world it requires prediction with
652 sparse data and fragmentary knowledge. Topographic information with high spatial resolution is freely
653 available globally, allowing us to implement the HSC model in global scale studies. In addition, thanks to
654 the recent development, testing, and validation of remote sensing evaporation products in large spatial
655 scale (e.g. Anderson et al., 2011; Hu and Jia, 2015), the S_{uMax} estimation has become possible without in

656 situ hydro-meteorological measurements (Wang-Erlandsson et al., 2016). These widely-accessible
657 datasets make the global-scale implementation of HSC-MCT module promising.

658 Although the new modules perform well in the BB and the MOPEX catchments, we do not intend to
659 propose “a model fits all”. The assumption of HSC, to some extent, is supported by large-sample ecological
660 field observation (Fan et al., 2017), but it never means the A_s - S_u curve of HSC can perfectly fit the other
661 existing curves (e.g. HBV and TOPMODEL). Unify all model approaches into one framework is the objective
662 of several pioneer works (e.g. Clark, et al., 2010; Fenicia et al., 2011), but out of the scope of this study.
663 Moreover, while estimating the runoff coefficient by the A_s - S_u relation, rainfall in the early time may cause
664 the increase of S_u/S_{uMax} and runoff coefficient (Moore, 1985; Wang, 2018). Therefore, neglecting this
665 influence factor, HBV (Equation 1), TOPMODEL (Equation 2-4) and HSC (Equation 5-6) theoretically
666 underestimate the runoff coefficient, which needs to be further investigated.

667 Finally, we should not ignore the limitations of the new module, although it has better performance and
668 modelling consistency. 1) The threshold area for the initiating a stream was set as a constant value for the
669 entire CONUS, but the variation of this value in different climate, geology and landscape classes
670 (Montgomery and Dietrich, 1989; Helmlinger et al., 1993; Colombo et al., 2007; Moussa, 2008) needs to
671 be future investigated. 2) The discrepancy between observed and simulated saturation area needs to be
672 further investigated, by utilizing more advanced field measurement and simultaneously refining the
673 model assumption. To our understanding, there are two interpretations. Firstly, the overestimation of the
674 HSC model is possibly because two runoff generation mechanisms – SOF and the SSF occur at the same
675 time. However, the saturated area observed by the “squishy boot” method (Ali et al., 2013), probably only
676 distinguished the areas where SOF occurred. Subsurface stormflow, also contributing to runoff, cannot be
677 observed by the “squishy boot” method. Thus, this mismatch between simulation and observation
678 probably leads to this saturated area overestimation. The second interpretation might be the different
679 definition of “saturation”. The observed saturated areas are places where 100% of soil pore volume is
680 filled by water. But the modelled saturation areas are located where soil moisture is above field capacity,
681 and not necessarily 100% filled with water, which probably also results in the overestimation of saturated
682 areas. Interestingly, in theory the observed saturated area should be within the simulated contributing
683 area, due to the fact that the saturated soil moisture is always larger than field capacity. From this point
684 of view, the observed saturated area is smaller and within the contributing area simulated by HSC, but
685 TOPMODEL missed this important feature. 4) Only the runoff generation module is calibration free, but
686 the interception and response routines still rely on calibration. Although we kept the interception and

687 response routine modules the same for the four models, the variation of other calibrated parameters (i.e.
688 S_{iMax} , D , K_f , K_s , T_{lagF}) may also influence model performance in both calibration and validation. 5) The
689 computational cost of the HSC is more expensive than HBV, and similar to TOPMODEL, due to the cost of
690 preprocessed topographic analysis. But once the S_u - A_s curve is completed, the computation cost is quite
691 comparable with HBV.

692 7 Summary and conclusions

693 In this study, we developed a simple and calibration-free hydrological module (HAND-based Storage
694 Capacity curve, HSC) based on a relatively new topographic index (HAND), which is not only an excellent
695 physically-based indicator for the hydraulic gradient, but also represents the spatial distribution of root
696 zone storage capacity supported by large-sample ecological observations. Based on HAND spatial
697 distribution pattern, the soil moisture (S_u) - saturated area (A_s) relation for each catchment was derived,
698 which was used to estimate the A_s of specific rainfall event based on continuous calculation of S_u .
699 Subsequently, based on the S_u - A_s relation, the HSC module was developed. Then, applying the mass curve
700 technique (MCT) approach, we estimated the root zone storage capacity (S_{uMax}) from observable hydro-
701 climatological and vegetation data, and coupled it with HSC to create the calibration-free HSC-MCT
702 module. The HBV and TOPMODEL were used as two benchmarks to test the performance of HSC and HSC-
703 MCT on both hydrograph simulation and ability to reproduce the contributing area, which was measured
704 for different hydrometeorological conditions in the Bruntland Burn catchment in Scotland. Subsequently,
705 323 MOPEX catchments in the US were used as a large-sample hydrological study to further validate the
706 effectiveness of our proposed runoff generation modules.

707 In the BB exploratory study, we found that the HSC, HBV and TOPMODEL performed comparably well to
708 reproduce the observed hydrograph. Comparing the estimated contributing area of TOPMODEL with the
709 HSC module, we found that HSC module performed better to reproduce saturated area variation, in terms
710 of the correlation coefficient and spatial patterns. This likely indicates that HAND maybe a better indicator
711 to distinguish hydrological similarity than TWI.

712 For the 323 MOPEX catchments, HSC improved the averaged validation value of I_{KGE} from 0.62 (HBV) and
713 0.61 (TOPMODEL) to 0.65. In 12% of the MOPEX catchments, the HSC module outperforms HBV, and in
714 not a single catchment did the calibrated HBV outperform the HSC. Comparing with TOPMODEL, the HSC
715 outperformed in 8% of the catchments, and in only 1% of catchments TOPMODEL has a better
716 performance. Interestingly, we found that the HSC module showed better performance in the catchments

717 with gentle topography, less forest cover, and larger aridity index. Not surprisingly, the I_{KGE} of HSC-MCT
718 model was slightly reduced to 0.59, due to the non-calibrated S_{uMax} , but still comparably well performed
719 as HBV (0.62) and TOPMODEL (0.61). This illustrates the robustness of both the HSC approach to derive
720 the spatial distribution of the root zone storage capacity (β) and the efficiency of the MCT method to
721 estimate the root zone storage capacity (S_{uMax}).

722

723 **Acknowledgement:**

724 This study was supported by National Natural Science Foundation of China (41801036), National Key R&D
725 Program of China (2017YFE0100700), the Key Program of National Natural Science Foundation of China
726 (No. 41730646), and Key Laboratory for Mountain Hazards and Earth Surface Process, Institute of
727 Mountain Hazards and Environment, Chinese Academy of Sciences (KLMHESP-17-02).

728

729 **Author contributions:**

730 H.G. and H.H.G.S. designed research; H.G. performed research; C.B., C.S., D.T and H.G. provided data,
731 among which the dynamics of the saturation areas data in the BB was provided by C.B. C.S., and D.T.; H.G.
732 analysed data; C.B. was involved in the interpretation of some of the modelling work in the BB; H.G. M.H,
733 and H.H.G.S. wrote the paper; CS and DT extensively edited the paper, and provided substantial comments
734 and constructive suggestions for scientific clarification.

735

736 **References:**

737 Anderson, M. C., Kustas, W. P., Norman, J. M., Hain, C. R., Mecikalski, J. R., Schultz, L., González-Dugo, M.
738 P., Cammalleri, C., D'Urso, G., Pimstein, A., and Gao, F.: Mapping daily evapotranspiration at field to
739 continental scales using geostationary and polar orbiting satellite imagery, *Hydrol. Earth Syst. Sci.*, 15,
740 223–239, doi:10.5194/hess-15-223-2011, 2011.

741 Andréassian V, Bourgin F, Oudin L, Mathevet T, Perrin C, Lerat J, Coron L, Berthet L.: Seeking genericity in
742 the selection of parameter sets: Impact on hydrological model efficiency. *Water Resources Research* 50
743 (10): 8356–8366, 2014.

744 Bergström S, Forsman A.: Development of a conceptual deterministic rainfall-runoff model. *Hydrology*
745 *Research* 4 (3): 147–170, 1973.

746 Bergström S, Lindström G.: Interpretation of runoff processes in hydrological modelling—experience from
747 the HBV approach. *Hydrological Processes* 29 (16): 3535–3545, 2015.

748 Beven K.: Robert E. Horton’s perceptual model of infiltration processes. *Hydrological Processes* 18 (17):
749 3447–3460 DOI: 10.1002/hyp.5740, 2004.

750 Beven K, Freer J.: A dynamic TOPMODEL. *Hydrological Processes* 15 (10): 1993–2011 DOI: 10.1002/hyp,
751 2001.

752 Beven K. 1993. Prophecy, reality and uncertainty in distributed hydrological modelling. *Advances in Water*
753 *Resources* 16 (1): 41–51 DOI: [http://dx.doi.org/10.1016/0309-1708\(93\)90028-E](http://dx.doi.org/10.1016/0309-1708(93)90028-E)

754 Beven K.: Linking parameters across scales: Subgrid parameterizations and scale dependent hydrological
755 models. *Hydrological Processes* 9 (September 1994): 507–525 DOI: 10.1002/hyp.3360090504.252, 1995.

756 Beven KJ.: *Rainfall–Runoff Models: The Primer*, 2012.

757 Beven K., Germann P.: Macropores and water-flow in soils. *Water Resour. Res.* 18, 1311–1325, 1982.

758 Beven KJ, Kirkby MJ.: A physically based, variable contributing area model of basin hydrology. *Hydrological*
759 *Sciences Bulletin* 24 (1): 43–69 DOI: 10.1080/02626667909491834, 1979.

760 Beven, K.: Changing ideas in hydrology – the case of physically-based models. *J. Hydrol.* 105 (1–2), 157–
761 172, 1989.

762 Birkel C, Tetzlaff D, Dunn SM, Soulsby C.: Towards a simple dynamic process conceptualization in rainfall –
763 runoff models using multi - criteria calibration and tracers in temperate, upland catchments. *Hydrological*
764 *Processes* 24 (3): 260 – 275, 2010.

765 Birkel, C., Soulsby, C., and Tetzlaff, D.: Conceptual modelling to assess how the interplay of hydrological
766 connectivity, catchment storage and tracer dynamics controls non-stationary water age estimates.
767 *Hydrological Processes*, DOI: 10.1002/hyp.10414, 2014.

768 Blöschl G.: *Runoff prediction in ungauged basins: synthesis across processes, places and scales*. Cambridge
769 University Press, 2013.

770 Brooks, R. J., Barnard, H. R., Coulombe, R. & McDonnell, J. J.: Ecohydrologic separation of water between
771 trees and streams in a Mediterranean climate. *Nature Geoscience* 3, 100–104. DOI: 10.1038/ngeo722,
772 2010.

773 Budyko M.I.: *Climate and life*, 1971.

774 Burt TP, McDonnell JJ.: Whither field hydrology? The need for discovery science and outrageous
775 hydrological hypotheses. *Water Resources Research* 51 (8): 5919–5928 DOI: 10.1002/2014WR016839,
776 2015.

777 Chase, CG.: Fluvial landsculpting and the fractal dimension of topography. *Geomorphology* 5 (1): 39–57
778 DOI: [http://dx.doi.org/10.1016/0169-555X\(92\)90057-U](http://dx.doi.org/10.1016/0169-555X(92)90057-U), 1992.

779 Clark, MP, Slater, AG, Rupp, DE, Woods, R A., Vrugt, J A., Gupta, H V., Wagener, T, Hay, LE.: Framework for
780 Understanding Structural Errors (FUSE): A modular framework to diagnose differences between
781 hydrological models. *Water Resources Research* 44: 1–14 DOI: 10.1029/2007WR006735, 2008.

782 Clark, M. P., Kavetski, D. and Fenicia, F.: Pursuing the Method of Multiple Working Hypotheses for
783 Hydrological Modeling. *Water Resources Research* 47.9: 1–16, 2011.

784 Colombo, R., Vogt, J. V., Soille, P., Paracchini, M. L., de Jager, A.: Deriving river networks and catchments
785 at the European scale from medium resolution digital elevation data. *CATENA* 70 (3): 296–305 DOI:
786 <http://doi.org/10.1016/j.catena.2006.10.001>, 2007.

787 Condon, Laura E, and Reed M Maxwell. “Evaluating the Relationship between Topography and
788 Groundwater Using Outputs from a Continental-Scale Integrated Hydrology Model.” *Water Resources*
789 *Research* 51.8 (2015): 6602–6621.

790 Duan, Q., Schaake, J., Andréassian, V., Franks, S., Goteti, G., Gupta, H. V., Gusev, Y.M, Habets, F., Hall, A.,
791 Hay, L., Model Parameter Estimation Experiment (MOPEX): An overview of science strategy and major
792 results from the second and third workshops. *Journal of Hydrology* 320 (1-2): 3–17 DOI:
793 10.1016/j.jhydrol.2005.07.031, 2006.

794 Dunne, T., Black, R.D.: Partial area contributions to Storm Runoff in a Small New England Watershed.
795 *Water Resources Research* 6 (5): 1296–1311, 1970.

796 Boer-Euser, T., McMillan, H. K., Hrachowitz, M., Winsemius, H. C., and Savenije, H. H. G.: Influence of soil
797 and climate on root zone storage capacity, *Water Resour. Res.*, 52, 2009–2024,
798 doi:10.1002/2015WR018115, 2016.

799 Fan, Y., Miguezmacho, G., Jobbágy, E. G., Jackson, R. B., & Oterocasal, C.: Hydrologic regulation of plant
800 rooting depth. *Proceedings of the National Academy of Sciences of the United States of America*, 114(40),
801 201712381, 2017.

802 Fenicia, F., Savenije, H.H.G., Matgen, P., Pfister, L.: A comparison of alternative multiobjective calibration
803 strategies for hydrological modeling. *Water Resources Research* 43 (3): n/a–n/a DOI:
804 10.1029/2006WR005098, 2007.

805 Gao, H., Hrachowitz, M., Schymanski, S.J., Fenicia, F., Sriwongsitanon, N., Savenije, H.H.G.: Climate
806 controls how ecosystems size the root zone storage capacity at catchment scale. *Geophysical Research*
807 *Letters* 41 (22): 7916–7923 DOI: 10.1002/2014gl061668, 2014a.

808 Gao, H., Hrachowitz, M., Fenicia, F., Gharari, S., Savenije, H.H.G.: Testing the realism of a topography-
809 driven model (FLEX-Topo) in the nested catchments of the Upper Heihe, China. *Hydrology and Earth*
810 *System Sciences* 18 (5): 1895–1915 DOI: 10.5194/hess-18-1895-2014, 2014b.

811 Gao, H., Hrachowitz, M., Sriwongsitanon, N., Fenicia, F., Gharari, S., Savenije, H.H.G.: Accounting for the
812 influence of vegetation and landscape improves model transferability in a tropical savannah region. *Water*
813 *Resources Research* 52 (10): 7999–8022 DOI: 10.1002/2016WR019574, 2016.

814 Gao, H., Sabo, J.L, Chen, X., Liu, Z., Yang, Z., Ren, Z., Liu, M.: Landscape heterogeneity and hydrological
815 processes: a review of landscape-based hydrological models. *Landscape Ecology*, DOI:
816 doi.org/10.1007/s10980-018-0690-4, 2018a.

817 Gao, H., Cai, H., Zheng, D.: Understand the impacts of landscape features on the shape of storage capacity
818 curve and its influence on flood. *Hydrology Research*. DOI: Hydrology-D-16-00245R3, 2018b.

819 Gao, J., Holden, J., Kirkby, M.: The impact of land-cover change on flood peaks in peatland basins. *Water*
820 *Resources Research* 52 (5): 3477–3492 DOI: 10.1002/2015WR017667, 2016.

821 Gharari, S., Hrachowitz, M., Fenicia, F., Savenije, H.H.G.: Hydrological landscape classification:
822 investigating the performance of HAND based landscape classifications in a central European meso-scale

823 catchment. *Hydrology and Earth System Sciences* 15 (11): 3275–3291 DOI: 10.5194/hess-15-3275-2011,
824 2011.

825 Gharari, S., Hrachowitz, M., Fenicia, F., Gao, H., Savenije, H.H.G.: Using expert knowledge to increase
826 realism in environmental system models can dramatically reduce the need for calibration. *Hydrology and*
827 *Earth System Sciences* 18 (12): 4839–4859 DOI: 10.5194/hess-18-4839-2014, 2014.

828 Gharari, S. On the role of model structure in hydrological modeling: Understanding models, PhD
829 dissertation, 2016

830 Gomes, G.J.C., Vrugt, J.A., Vargas, E.A.: Toward improved prediction of the bedrock depth underneath
831 hillslopes: Bayesian inference of the bottom-up control hypothesis using high-resolution topographic data.
832 *Water Resources Research* 52 (4): 3085–3112 DOI: 10.1002/2015WR018147, 2016.

833 Grabs, T., Seibert, J., Bishop, K., Laudon, H.: Modeling spatial patterns of saturated areas: A comparison
834 of the topographic wetness index and a dynamic distributed model. *Journal of Hydrology* 373 (1): 15–23,
835 2009.

836 De Groen, M.M., Savenije, H.H.G.: A monthly interception equation based on the statistical characteristics
837 of daily rainfall. *Water Resources Research* 42 (12): n/a–n/a DOI: 10.1029/2006WR005013, 2006.

838 Gumbel, E. J.: Les valeurs extrêmes des distributions statistiques, *Annales de l’institut Henri Poincaré*, 5(2),
839 115–158, 1935.

840 Gupta, H. V., Kling, H., Yilmaz, K.K., Martinez, G.F.: Decomposition of the mean squared error and NSE
841 performance criteria: Implications for improving hydrological modelling. *Journal of Hydrology* 377 (1-2):
842 80–91 DOI: 10.1016/j.jhydrol.2009.08.003, 2009.

843 Hargreaves, G.H., Samani, Z.A.: Reference crop evapotranspiration from temperature. *Applied*
844 *engineering in agriculture* 1 (2): 96–99, 1985.

845 Haria, A.H., Shand, P.: Evidence for deep sub-surface flow routing in forested upland Wales: implications
846 for contaminant transport and stream flow generation. *Hydrology and Earth System Sciences Discussions*
847 8 (3): 334–344, 2004.

848 Harte, J.: Toward a synthesis of the Newtonian and Darwinian worldviews. *Physics Today* 55 (10): 29–34
849 DOI: 10.1063/1.1522164, 2002.

850 Helmlinger, K.R., Kumar, P., Foufoula-Georgiou, E.: On the use of digital elevation model data for
851 Hortonian and fractal analyses of channel network. *Water Resources Research* 29: 2599–2613, 1993.

852 Hewlett, J.D.: Soil moisture as a source of base flow from steep mountain watersheds. Southeastern Forest
853 Experiment Station, US Department of Agriculture, Forest Service, 1961.

854 Hewlett, J.D., Troendle, C.A.: Non point and diffused water sources: a variable source area problem. In
855 *Watershed Management; Proceedings of a Symposium*, 1975.

856 Homer, C. G., Dewitz, J. A., Yang, L., Jin, S., Danielson, P., Xian, G., Coulston, J., Herold, N. D., Wickham, J.
857 D. & Megown, K.: Completion of the 2011 National Land Cover Database for the conterminous United
858 States-representing a decade of land cover change information. *Photogrammetric Engineering and*
859 *Remote Sensing* 81, 345–354, 2015.

860 Hooshyar, M., Wang, D., Kim, S., Medeiros, S.C., Hagen, S.C.: Valley and channel networks extraction based
861 on local topographic curvature and k - means clustering of contours. *Water Resources Research* 52 (10):
862 8081 – 8102, 2016.

863 Horton, R.E.: The role of infiltration in the hydrologic cycle. *Trans. Am. Geophys. Union* 14, 446–460, 1933.

864 Hrachowitz, M., Savenije, H.H.G., Blöschl, G., McDonnell, J.J., Sivapalan, M., Pomeroy, J.W., Arheimer, B.,
865 Blume, T., Clark, M.P., Ehret, U., Fenicia, F., Freer, J.E., Gelfan, A., Gupta, H.V., Hughes, D.A., Hut, R.W.,
866 Montanari, A., Pande, S., Tetzlaff, D., Troch, P.A., Uhlenbrook, S., Wagener, T., Winsemius, H.C., Woods,
867 R.A., Zehe E., & Cudennec, C.: . A decade of Predictions in Ungauged Basins (PUB)—a review. *Hydrological*
868 *Sciences Journal* 58 (6): 1198–1255 DOI: 10.1080/02626667.2013.803183, 2013.

869 [Hrachowitz, M. and Clark, M. P.: HESS Opinions: The complementary merits of competing modelling](https://doi.org/10.5194/hess-21-3953-2017)
870 [philosophies in hydrology, *Hydrol. Earth Syst. Sci.*, 21, 3953-3973, https://doi.org/10.5194/hess-21-3953-](https://doi.org/10.5194/hess-21-3953-2017)
871 [2017, 2017.](https://doi.org/10.5194/hess-21-3953-2017)

872 Hu, G. and Jia, L.: Monitoring of evapotranspiration in a semiarid inland river basin by combining
873 microwave and optical remote sensing observations, *Remote Sens.*, 7, 3056–3087,
874 doi:10.3390/rs70303056, 2015.

875 Iorgulescu, I., Jordan, J-P.: Validation of TOPMODEL on a small Swiss catchment. *Journal of Hydrology* 159
876 (1): 255–273 DOI: [http://dx.doi.org/10.1016/0022-1694\(94\)90260-7](http://dx.doi.org/10.1016/0022-1694(94)90260-7), 1994.

877 Kirchner, J.W.: Getting the right answers for the right reasons: Linking measurements, analyses, and
878 models to advance the science of hydrology. *Water Resources Research* 42 (3): n/a–n/a DOI:
879 10.1029/2005WR004362, 2006.

880 Kleidon, A., Lorenz, R.D.: *Non-equilibrium thermodynamics and the production of entropy: life, earth, and*
881 *beyond*. Springer Science & Business Media, 2004.

882 Kollat, J. B., P. M. Reed, and T. Wagener.: When are multiobjective calibration trade - offs in hydrologic
883 models meaningful?. *Water Resources Research* 48.3:3520, 2012.

884 Liang, X., Lettenmaier, D.P., Wood, E.F., Burges, S.J.: A simple hydrologically based model of land surface
885 water and energy fluxes for general circulation models. *Journal of Geophysical Research* 99 (D7): 14415
886 DOI: 10.1029/94JD00483, 1994.

887 Liu, D., Tian, F., Hu, H., Hu, H.: The role of run-on for overland flow and the characteristics of runoff
888 generation in the Loess Plateau, China. *Hydrological Sciences Journal* 57 (6): 1107–1117 DOI:
889 10.1080/02626667.2012.695870, 2012.

890 Maxwell, R. M., and Condon, L. E.: Connections between Groundwater Flow and Transpiration Partitioning.
891 *Science* 353.6297: 377 LP – 380, 2016.

892 McDonnell, J.J., Sivapalan, M., Vaché, K., Dunn, S., Grant, G., Haggerty, R., Hinz, C., Hooper, R., Kirchner,
893 J., Roderick, M.L., Selker, J. and Weiler, M.: Moving beyond heterogeneity and process complexity: A new
894 vision for watershed hydrology. *Water Resources Research* 43 (7): n/a–n/a DOI: 10.1029/2006WR005467,
895 2007.

896 McDonnell, J.J.: Are all runoff processes the same? *Hydrological Processes* 27 (26): 4103–4111 DOI:
897 10.1002/hyp.10076, 2013.

898 Merz, R., Blöschl, G.: Regionalisation of catchment model parameters. *Journal of Hydrology* 287 (1-4): 95–
899 123 DOI: 10.1016/j.jhydrol.2003.09.028, 2004.

900 Milly, P. C. D.: Climate, soil water storage, and the average annual water balance, *Water Resour. Res.*,
901 30(7), 213–2156, 1994.

902 Molenat, J., Gascuel-Oudou, C., Ruiz, L., Gruau, G.: Role of water table dynamics on stream nitrate export
903 and concentration in agricultural headwater catchment (France). *Journal of Hydrology* 348 (3): 363–378,
904 2008.

905 Molé nat, J., Gascuel - Odoux, C., Davy, P., Durand, P.: How to model shallow water - table depth
906 variations: the case of the Kervidy - Naizin catchment, France. *Hydrological Processes* 19 (4): 901 - 920,
907 2005.

908 Montgomery, D.R., Dietrich, W.E.: Source areas, drainage density, and channel initiation. *Water Resources*
909 *Research* 25 (8): 1907–1918, 1989.

910 Moore, R. J.: The probability-distributed principle and runoff production at point and basin scales, *Hydrol.*
911 *Sci. J.*, 30, 273-297, 1985.

912 Moussa, R.: Effect of channel network topology, basin segmentation and rainfall spatial distribution on
913 the geomorphologic instantaneous unit hydrograph transfer function. *Hydrological Processes* 22 (3): 395–
914 419 DOI: 10.1002/hyp.6612, 2008.

915 Moussa, R.: Definition of new equivalent indices of Horton-Strahler ratios for the derivation of the
916 Geomorphological Instantaneous Unit Hydrograph. *Water Resources Research* 45 (9): n/a–n/a DOI:
917 10.1029/2008WR007330, 2009.

918 Nobre, A. D, Cuartas, L. A., Hodnett, M., Rennó, C.D., Rodrigues, G., Silveira, A., Waterloo, M., Saleska, S.:
919 Height Above the Nearest Drainage - a hydrologically relevant new terrain model. *Journal of Hydrology*
920 404 (1-2): 13–29 DOI: 10.1016/j.jhydrol.2011.03.051, 2011.

921 Orth, R., Staudinger, M., Seneviratne, S.I., Seibert, J., Zappa, M.: Does model performance improve with
922 complexity? A case study with three hydrological models. *Journal of Hydrology* 523: 147–159 DOI:
923 <http://doi.org/10.1016/j.jhydrol.2015.01.044>, 2015.

924 Passalacqua, P., Belmont, P., Staley, D.M., Simley, J.D., Arrowsmith, J.R., Bode, C.A., Crosby, C., DeLong,
925 S.B., Glenn, N.F., Kelly, S.A., Lague, D., Sangireddy, H., Schaffrath, K., Tarboton, D. G., Wasklewicz, T.,
926 Wheaton, J. M.: Analyzing high resolution topography for advancing the understanding of mass and
927 energy transfer through landscapes: A review. *Earth-Science Reviews* 148: 174–193 DOI:
928 <http://doi.org/10.1016/j.earscirev.2015.05.012>, 2015.

929 Pelletier, J.D., Barron-Gafford, G.A., Breshears, D.D., Brooks, P.D., Chorover, J., Durcik, M., Harman, C.J.,
930 Huxman, T.E., Lohse, K.A., Lybrand, R., Meixner, T., McIntosh, J. C., Papuga, S. A., Rasmussen, C., Schaap,
931 M., Swetnam, T. L., and Troch, P. A.: Coevolution of nonlinear trends in vegetation, soils, and topography
932 with elevation and slope aspect: A case study in the sky islands of southern Arizona. *Journal of Geophysical*
933 *Research: Earth Surface* 118 (2): 741–758 DOI: 10.1002/jgrf.20046, 2013.

934 Perrin, C., Michel, C., Andréassian, V.: Does a large number of parameters enhance model performance?
935 Comparative assessment of common catchment model structures on 429 catchments. *Journal of*
936 *Hydrology* 242 (3-4): 275–301 DOI: 10.1016/S0022-1694(00)00393-0, 2001.

937 Perrin, C., C. Michel, and V. Andréassian: Improvement of a parsimonious model for streamflow
938 simulation, *J. Hydrol.*, 279, 275– 289, 2003.

939 Ponce, V. M., and Hawkins, R. H.: Runoff curve number: Has it reached maturity?, *J. Hydrol. Eng.*, 1(1), 11–
940 19, 1996.

941 Rempe, D. M., and Dietrich, W. E.: A bottom-up control on fresh-bedrock topography under landscapes,
942 *Proc. Natl. Acad. Sci. U. S. A.*, 111(18), 6576–6581, doi:10.1073/pnas.1404763111, 2014.

943 Renard, K. G., Yoder, D. C., Lightle, D. T. & Dabney, S. M. Universal soil loss equation and revised universal
944 soil loss equation. *Handbook of Erosion Modelling* 8, 135–167, 2011.

945 Rennó, C.D., Nobre, A.D., Cuartas, L.A., Soares, J.V., Hodnett, M.G., Tomasella, J., Waterloo, M. HAND, a
946 new terrain descriptor using SRTM-DEM; mapping terra-firme rainforest environments in Amazonia.
947 *Remote Sensing of Environment* 112, 3469–3481, 2008.

948 Rodriguez-Iturbe, I., and A. Rinaldo, *Fractal River Basins: Chance and Self-Organization*, Cambridge Univ.
949 Press, 547 pp., New York, 1997.

950 Samaniego, L., Kumar, R., Attinger, S.: Multiscale parameter regionalization of a grid-based hydrologic
951 model at the mesoscale. *Water Resources Research* 46 (5): n/a–n/a DOI: 10.1029/2008WR007327, 2010.

952 Savenije, H. H. G.: HESS Opinions “Topography driven conceptual modelling (FLEX-Topo)”, *Hydrol. Earth*
953 *Syst. Sci.*, 14, 2681–2692, doi:10.5194/hess-14-2681-2010, 2010.

954 Savenije, H.H.G., Hrachowitz, M.: HESS Opinions ‘Catchments as meta-organisms – a new blueprint for
955 hydrological modelling’. *Hydrol. Earth Syst. Sci.* 21 (2): 1107–1116 DOI: 10.5194/hess-21-1107-2017, 2017.

956 Schaake, J., Cong, S., and Duan, Q.: The US MOPEX data set, *IAHS Publ.*, 307, 9, 2006.

957 Schwarz, G. E. & Alexander, R. B. *State Soil Geographic (STATSGO) Data Base for the Conterminous United*
958 *States*. Open File report 95-449, US Geological Survey, Washington, DC, 1995.

959 Seibert, J., Stendahl, J., Sørensen, R.: Topographical influences on soil properties in boreal forests.
960 *Geoderma* 141 (1-2): 139–148 DOI: 10.1016/j.geoderma.2007.05.013, 2007.

961 Shao, W., Su, Y., and Langhammer, J.: Simulations of coupled non-isothermal soil moisture transport and
962 evaporation fluxes in a forest area. *Journal of Hydrology and Hydromechanics*, 65, 410–425, 2018

963 Shand, P., Haria, A.H., Neal, C., Griffiths, K., Gooddy, D., Dixon, A.J., Hill, T., Buckley, D.K., Cunningham, J.:
964 Hydrochemical heterogeneity in an upland catchment: further characterisation of the spatial, temporal
965 and depth variations in soils, streams and groundwaters of the Plynlimon forested catchment, Wales.
966 *Hydrology and Earth System Sciences* 9 (6): 621–644, 2005.

967 Sørensen, R., Seibert, J.: Effects of DEM resolution on the calculation of topographical indices: TWI and its
968 components. *Journal of Hydrology* 347 (1): 79–89 DOI: <http://dx.doi.org/10.1016/j.jhydrol.2007.09.001>,
969 2007.

970 Sivapalan, M., Woods, R.A., Kalma, J.D.: Variable bucket representation of TOPMODEL and investigation
971 of the effects of rainfall heterogeneity. *Hydrological processes* 11 (9): 1307–1330, 1997.

972 Sivapalan, M., Takeuchi, K., Franks, S.W., Gupta, V.K., Karambiri, H., Lakshmi, V., Liang, X., McDonnell, J.J.,
973 Mendiondo, E.M., O’Connell, P.E., Oki, T., Pomeroy, J. W., Schertzer, D., Uhlenbrook, S., Zehe, E.: IAHS
974 Decade on Predictions in Ungauged Basins (PUB), 2003–2012: Shaping an exciting future for the
975 hydrological sciences. *Hydrological Sciences Journal* 48 (6): 857–880 DOI: 10.1623/hysj.48.6.857.51421,
976 2003.

977 Sivapalan, M.: The secret to ‘doing better hydrological science’: change the question! *Hydrological*
978 *Processes* 23 (9): 1391–1396 DOI: 10.1002/hyp.7242, 2009.

979 Sivapalan, M., Blöschl, G.: Time scale interactions and the coevolution of humans and water. *Water*
980 *Resources Research* 51 (9): 6988–7022 DOI: 10.1002/2015WR017896, 2015.

981 Soulsby, C., Birkel, C., Geris, J., Dick, J., Tunaley, C. and Tetzlaff, D.: Stream water age distributions
982 controlled by storage dynamics and non-linear hydrologic connectivity: modelling with high resolution
983 isotope data. *Water Resources Research*. DOI: 10.1002/2015WR017888, 2015.

984 Soulsby, C., Bradford, J., Dick, J., McNamara, J.P., Geris, J., Lessels, J., Blumstock, M., Tetzlaff, D.: Using
985 geophysical surveys to test tracer-based storage estimates in headwater catchments. *Hydrological*
986 *Processes* 30 (23): 4434–4445 DOI: 10.1002/hyp.10889, 2016.

987 Sklash, M.G., Farvolden, R.N.: The role of groundwater in storm runoff. *Journal of Hydrology* 43 (1): 45–
988 65 DOI: [http://dx.doi.org/10.1016/0022-1694\(79\)90164-1](http://dx.doi.org/10.1016/0022-1694(79)90164-1), 1979.

989 Tetzlaff, D., Birkel, C., Dick, J., and C. Soulsby: Storage dynamics in hydrogeological units control hillslope
990 connectivity, runoff generation and the evolution of catchment transit time distributions. *Water*
991 *Resources Research*, DOI: 10.1002/2013WR014147, 2014.

992 Tian, F. Q. , Hu, H. P. , & Lei, Z. D.: Thermodynamic watershed hydrological model: constitutive relationship.
993 *Science in China Series E: Technological Sciences*, 51(9), 1353-1369, 2008. Troch, P. A., Carrillo, G.,
994 Sivapalan, M., Wagener, T., Sawicz, K.: Climate-vegetation-soil interactions and long-term hydrologic
995 partitioning: signatures of catchment co-evolution. *Hydrology and Earth System Sciences* 17 (6): 2209–
996 2217 DOI: 10.5194/hess-17-2209-2013, 2013.

997 Tromp-van Meerveld, H. J. & McDonnell, J. J.: Threshold relations in subsurface stormflow: 1. A 147-storm
998 analysis of the Panola hillslope. *Water Resources Research* 42. DOI: 10.1029/2004WR003778, 2006.

999 Van Beek, L.P.H. and M.F.P. Bierkens, The Global Hydrological Model PCR-GLOBWB: Conceptualization,
1000 Parameterization and Verification, Report Department of Physical Geography, Utrecht University, Utrecht,
1001 The Netherlands, <http://vanbeek.geo.uu.nl/suppinfo/vanbeekbierkens2009.pdf>, 2008.

1002 Vrugt, J. A.: Effective and efficient algorithm for multiobjective optimization of hydrologic models. *Water*
1003 *Resources Research* 39 (8): 1–19 DOI: 10.1029/2002WR001746, 2003.

1004 Wang, D., Tang, Y.: A one - parameter Budyko model for water balance captures emergent behavior in
1005 darwinian hydrologic models. *Geophysical Research Letters* 41 (13): 4569 – 4577, 2014.

1006 Wang, D.: A new probability density function for spatial distribution of soil water storage capacity leads
1007 to SCS curve number method, *Hydrol. Earth Syst. Sci. Discuss.*, <https://doi.org/10.5194/hess-2018-32>, in
1008 review, 2018.

1009 Wang-Erlandsson, L., Bastiaanssen, W.G.M., Gao, H., Jägermeyr, J., Senay, G.B., van Dijk, A.I.J.M.,
1010 Guerschman, J.P., Keys, P.W., Gordon, L.J., Savenije, H.H.G.: Global root zone storage capacity from
1011 satellite-based evaporation. *Hydrol. Earth Syst. Sci.* 20 (4): 1459–1481 DOI: 10.5194/hess-20-1459-2016,
1012 2016.

1013 Weiler, M., McDonnell, J. J.: Conceptualizing lateral preferential flow and flow networks and simulating
1014 the effects on gauged and ungauged hillslopes. *Water Resour. Res.* 43, W03403, 2007.

1015 Wolock, D. M.: STATSGO Soil Characteristics for the Conterminous United States. US Geological Survey,
1016 Washington, DC., 1997.

1017 Ye, A., Duan, Q., Yuan, X., Wood, E.F., Schaake, J.: Hydrologic post-processing of MOPEX streamflow
1018 simulations. *Journal of Hydrology* 508: 147–156 DOI: 10.1016/j.jhydrol.2013.10.055, 2014.

1019 Yu, Z., Lu, Q., Zhu, J., Yang, C., Ju, Q., Yang, T., Chen, X., and Sudicky, E. A.: Spatial and temporal scale effect
1020 in simulating hydrologic processes in a watershed. *Journal of Hydrologic Engineering*, 19(1), 99-107, 2014.

1021 Zehe, E., Fluehler, H.: Preferential transport of Isoproturon at a plot scale and a field scale tile-drained site.
1022 *J. Hydrol.* 247, 100–115, 2001.

1023 Zehe, E., Ehret, U., Blume, T., Kleidon, A., Scherer, U., Westhoff, M.: A thermodynamic approach to link
1024 self-organization, preferential flow and rainfall-runoff behaviour. *Hydrol. Earth Syst. Sci.* 17 (11): 4297–
1025 4322 DOI: 10.5194/hess-17-4297-2013, 2013.

1026 Zhao, R-J., Zuang, Y., Fang, L., Liu, X., Zhang, Q.: The Xinanjiang model. *Hydrological forecasting —*
1027 *Prévisions hydrologiques* (129): 351–356, 1980.

1028
1029
1030 Table 1. The parameters of the models, and their prior ranges for calibration. (* S_{uMax} is a parameter in HBV,
1031 TOPMODEL and the HSC model, but HSC-MCT model does not have S_{uMax} as a free parameter; ** β is a parameter in
1032 HBV model, but not in TOPMODEL, HSC and HSC-MCT models)

Parameter	Explanation	Prior range for calibration
S_{iMax} (mm)	Maximum interception capacity	2
S_{uMax} (mm) *	The root zone storage capacity	(10, 1000)
β (-)**	The shape of the storage capacity curve	(0.01, 5)
C_e (-)	Soil moisture threshold for reduction of evaporation	(0.1, 1)
D (-)	Splitter to fast and slow response reservoirs	(0, 1)
T_{lagF} (d)	Lag time from rainfall to peak flow	(0, 10)
K_f (d)	The fast recession coefficient	(1, 20)
K_s (d)	The slow recession coefficient	(20, 400)

1034

1035 Table 2. The water balance and constitutive equations used in models. (Function (15)* is used in the HBV model, but
 1036 not used in the TOPMODEL, HSC and HSC-MCT models)

reservoirs	Water balance equations	Constitutive equations
Interception reservoir	$\frac{dS_i}{dt} = P - E_i - P_e$ (8)	$E_i = \begin{cases} E_p; S_i > 0 \\ 0; S_i = 0 \end{cases} \quad (9)$ $P_e = \begin{cases} 0; S_i < S_{iMax} \\ P; S_i = S_{iMax} \end{cases} \quad (10)$
Unsaturated reservoir	$\frac{dS_u}{dt} = P_e - E_a - R_u$ (11)	$\frac{R_u}{P_e} = \left(\frac{S_u}{S_{uMax}} \right)^\beta \quad (12)^*$ $\frac{E_a}{E_p - E_i} = \frac{S_u}{C_e S_{uMax}} \quad (13)$
Splitter and Lag function		$R_f = R_u D \quad (17); R_s = R_u (1 - D) \quad (14)$ $R_{fl}(t) = \sum_{i=1}^{T_{lagf}} c_f(i) \cdot R_f(t - i + 1) \quad (15)$ $c_f(i) = i / \sum_{u=1}^{T_{lagf}} u \quad (16)$
Fast reservoir	$\frac{dS_f}{dt} = R_f - Q_f$ (17)	$Q_f = S_f / K_f$ (18)
Slow reservoir	$\frac{dS_s}{dt} = R_s - Q_s$ (19)	$Q_s = S_s / K_s$ (20)

1037

1038 Table 3. Data source of the MOPEX catchments.

Data	Unit	Resources	Website	Reference
Daily precipitation	mm/d	MOPEX	http://www.nws.noaa.gov/ohd/mopex/mo_datasets.htm	(Duan et al., 2006)
Daily maximum temperature	°C	MOPEX	Same as above	Same as above

Daily minimum temperature	°C	MOPEX	Same as above	Same as above
Daily runoff	mm/d	MOPEX	Same as above	Same as above
Aridity index	-	MOPEX	Same as above	Same as above
DEM	m	USGS	http://earthexplorer.usgs.gov/	-
Slope	degree	USGS	Same as above	-
K factor of soil	-	USGS	http://water.usgs.gov/GIS/metadata/usgswrd/XML/muid.xml	(Wolock, 1997; Gao et al., 2018)
Percentage of forest cover	%	NLCD	http://www.mrlc.gov/	(Homer et al., 2015; Gao et al., 2018)
Stream density	Km/km ²	Horizon Systems Corporation	http://www.horizon-systems.com/nhdplus/	-
Depth to bedrock	cm	STATSGO	http://www.soilinfo.psu.edu/index.cgi?soil_data&conus&data_code=v&dtb	(Schwarz et al., 1995; Gao et al., 2018)

1039

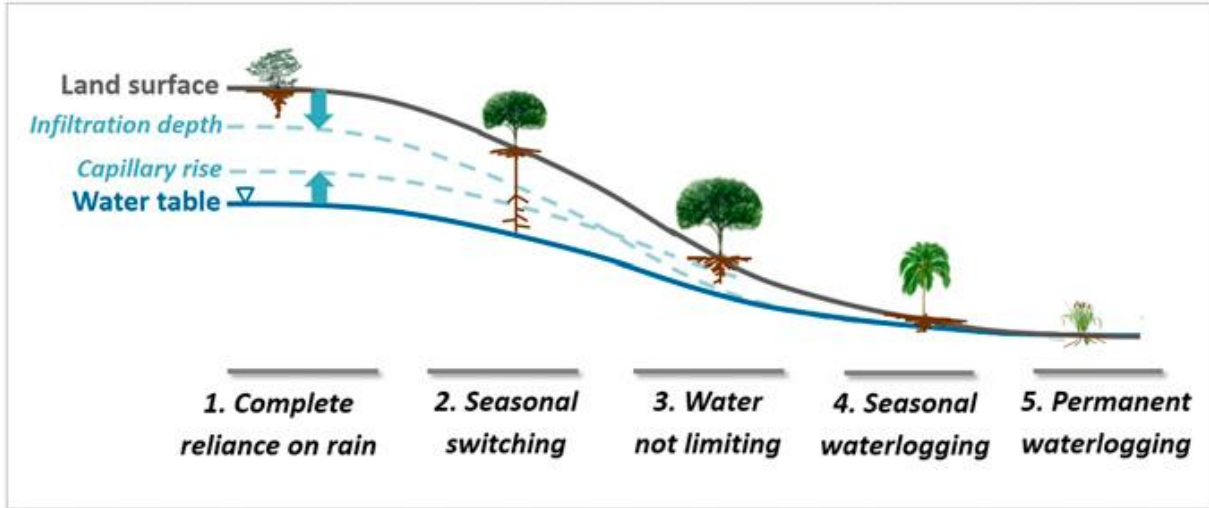
1040

1041 Table 4. Impacts of MOPEX catchment characteristics on model performance (HSC, HBV, and TOPMODEL)

Catchment characteristics	HSC > HBV	HSC ≈ HBV	HSC < HBV	HSC > TOPMODEL	HSC ≈ TOPMODEL	HSC < TOPMODEL
Averaged						
HAND (m)	37	71	-	27	69	193
Averaged slope (degree)	4.0	5.7	-	3.6	5.6	13.5
Averaged elevation (m)	454	395	-	469	393	740
Averaged K-factor (-)	0.28	0.29	-	0.29	0.29	0.25
Forest proportion (%)	22	43	-	14	43	68
Aridity index (-)	1.1	0.9	-	1.3	0.9	0.8
Stream density (-)	0.72	0.81	-	0.77	0.80	0.83

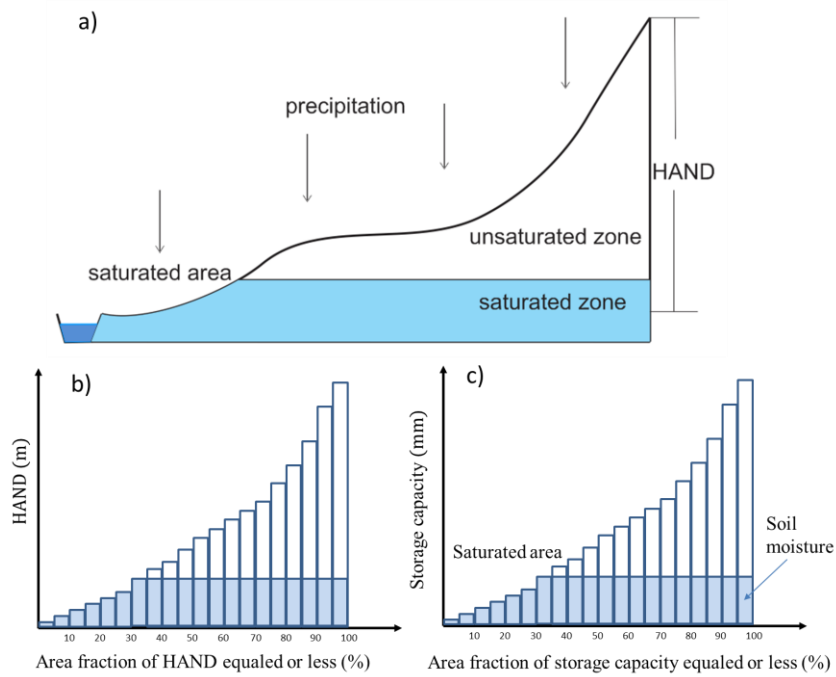
Averaged						
depth to rock						
(cm)	192	219	-	210	215	333

1042



1043

1044 Figure 1. The variation of plant rooting depths along a hillslope profile, showing the impact of HAND
 1045 (Height Above the Nearest Drainage) on rooting depth. (Taken from Fan et al., 2017 by permission of PNAS)



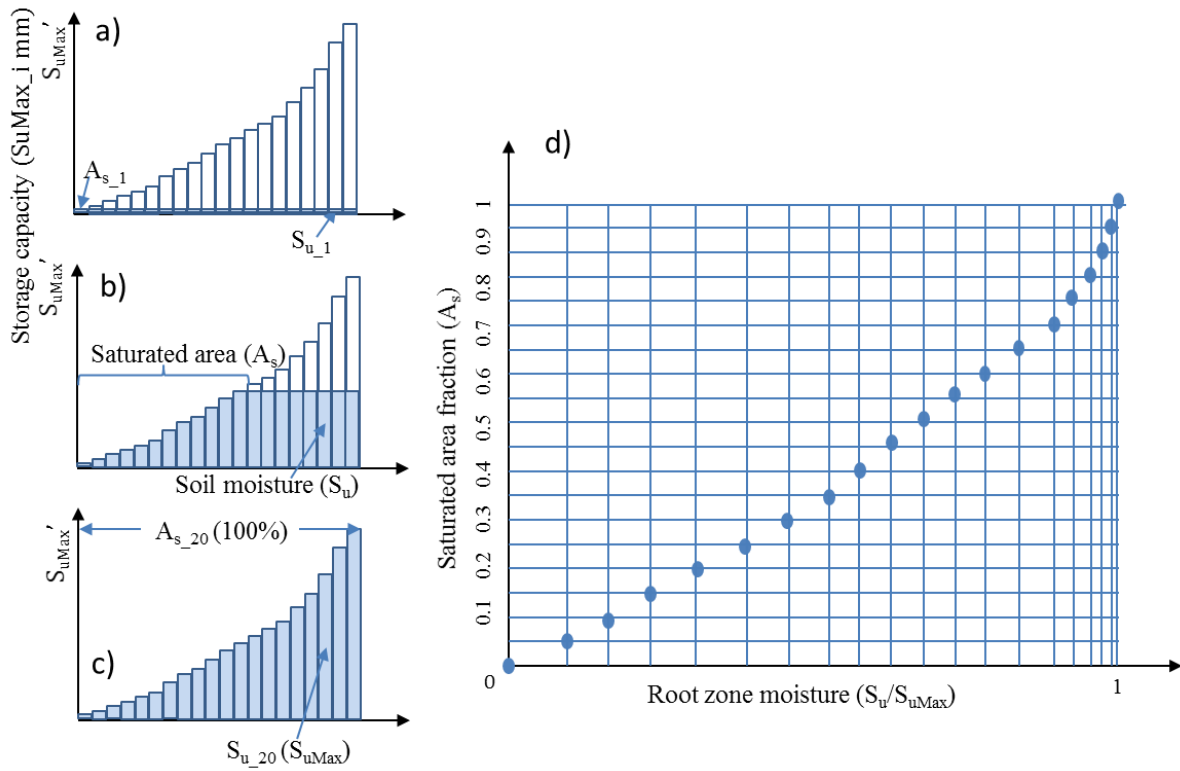
1046

1047 Figure 2. The perceptual model of the HAND-based Storage Capacity curve (HSC) model. a) shows the representative
 1048 hillslope profile in nature, and the saturated area, unsaturated zone and saturated zone; b) shows the relationship

1049 between HAND bands and their corresponded area fraction; c) shows the relationship between storage capacity-
 1050 area fraction-soil moisture-saturated area, based on the assumption that storage capacity linearly increases with
 1051 HAND values.

1052

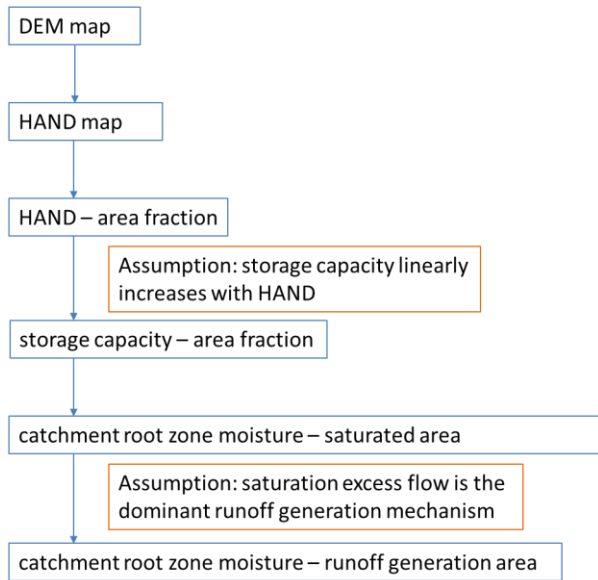
1053



1054

1055 Figure 3. The conceptual model of the HSC model. a), b) and c) illustrate the relationship between soil moisture (S_u)
 1056 and saturated area (A_s) in different soil moisture conditions. In d), 20 different S_u - A_s conditions are plotted, which
 1057 allow us to estimate A_s from S_u .

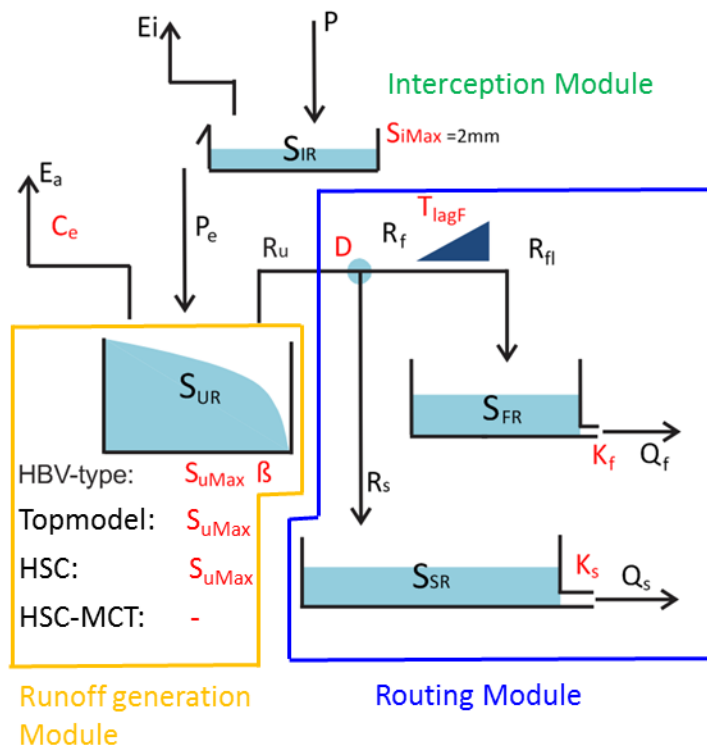
1058



1059

1060 Figure 4. The procedures estimating runoff generation by the HSC model and its two hypotheses.

1061



1062

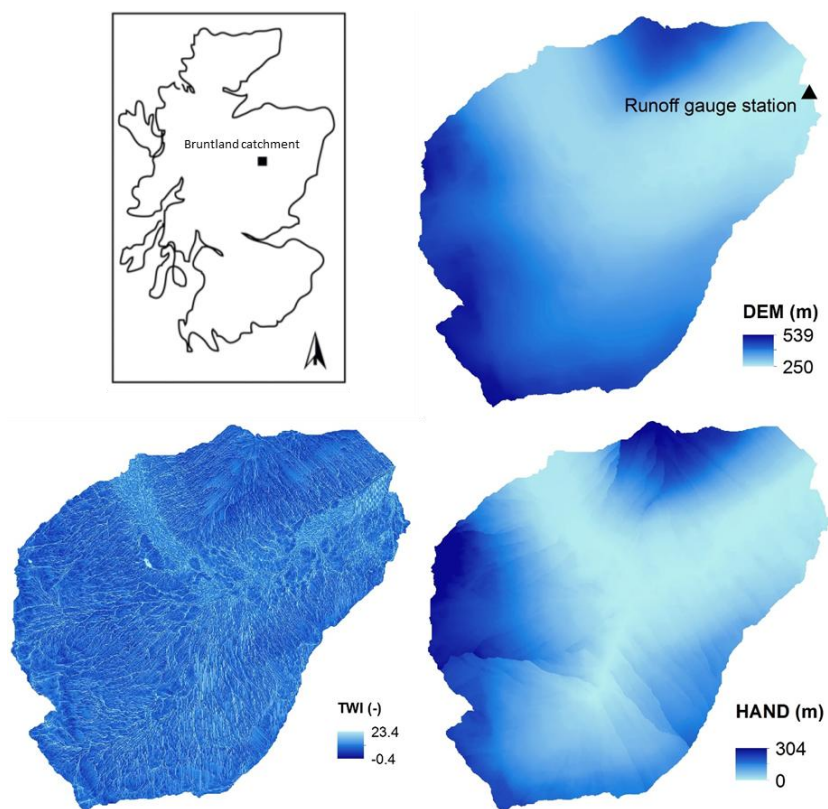
1063 Figure 5. Model structure and free parameters, involving four runoff generation models (HBV-type, TOPMODEL, HSC,

1064 and HSC -MCT). HBV-type has S_{uMax} and beta two free parameters; TOPMODEL and HSC models have S_{uMax} as one

1065 free parameter; and HSC-MCT model does not have free parameter. In order to simplify calibration process and
1066 make fair comparison, the interception storage capacity (S_{iMax}) was fixed as 2mm.

1067

1068

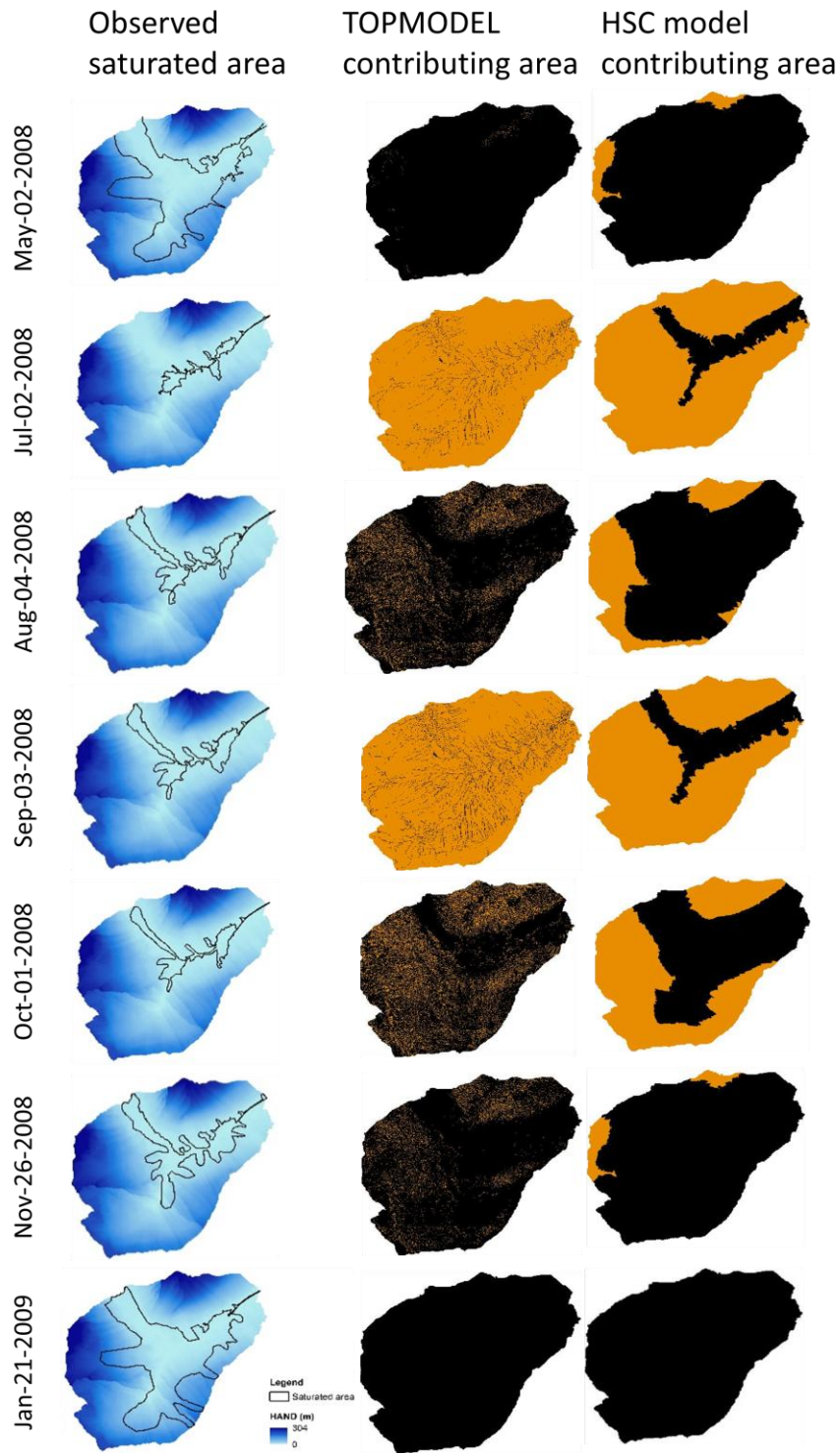


1069

1070 Figure 6. (a) Study site location of the Bruntland Burn catchment within Scotland; (b) digital elevation model (DEM)
1071 of the Bruntland Burn catchment; (c) the topographic wetness index map of the Bruntland Burn catchment; (d) the
1072 height above the nearest drainage (HAND) map of the Bruntland Burn catchment.

1073

1074

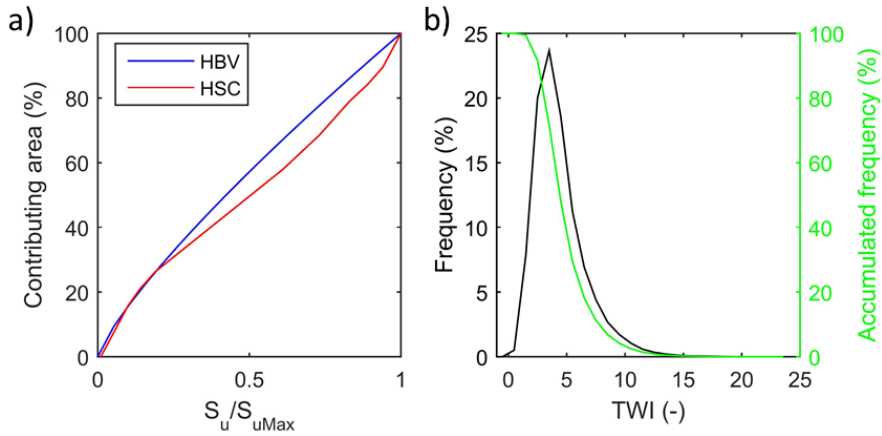


1075

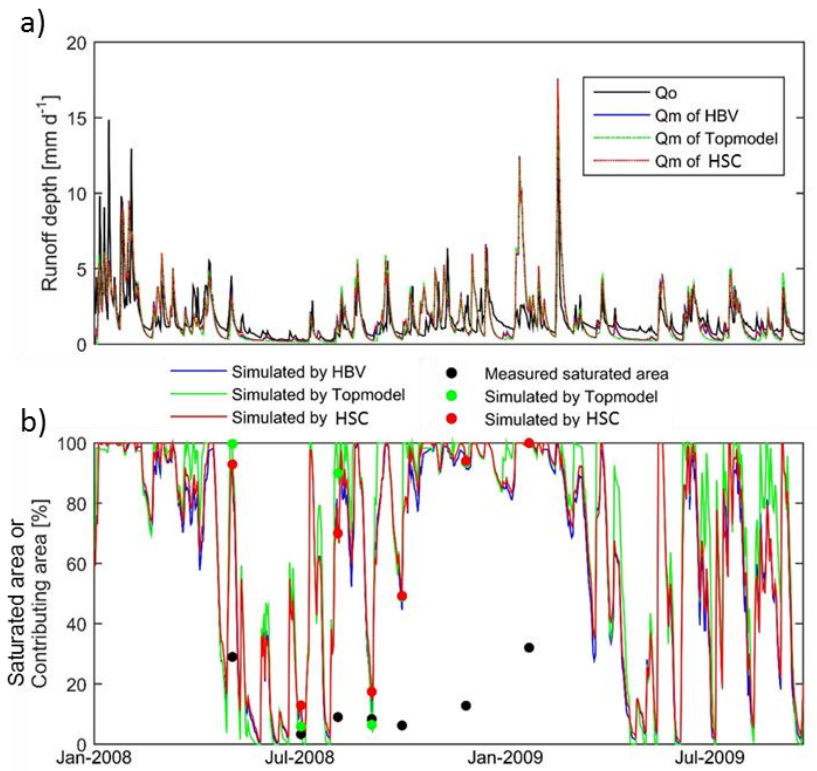
1076 Figure 7. The measured saturated areas and the simulated contributing areas (black) by TOPMODEL and HSC models.

1077

1078



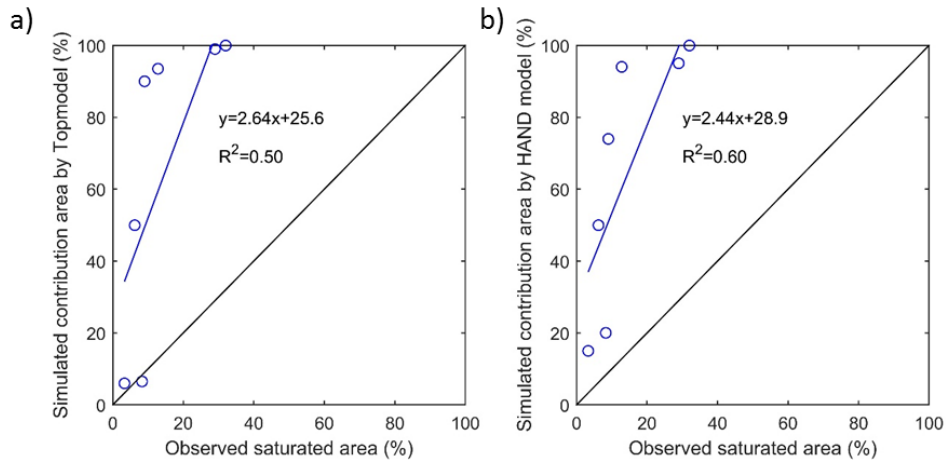
1079
 1080 Figure 8. The curves of the beta function of HBV model, and the S_u - A_s curve generated by HSC model (the left figure).
 1081 The frequency and accumulated frequency of the TWI in the Bruntland Burn catchment (the right figure).
 1082



1083
 1084 Figure 9. a) The observed hydrograph (Q_o , black line) of the Bruntland Burn catchment in 2008. And the simulated
 1085 hydrographs (Q_m) by HBV model (blue line), TOPMODEL (green dash line), HSC model (red dash line); b) the
 1086 comparison of the observed saturated area of 7 days (black dots) and simulated relative soil moistures, i.e. HBV (blue
 1087 line), TOPMODEL (green line and dots), HSC (red line and dots).

1088

1089



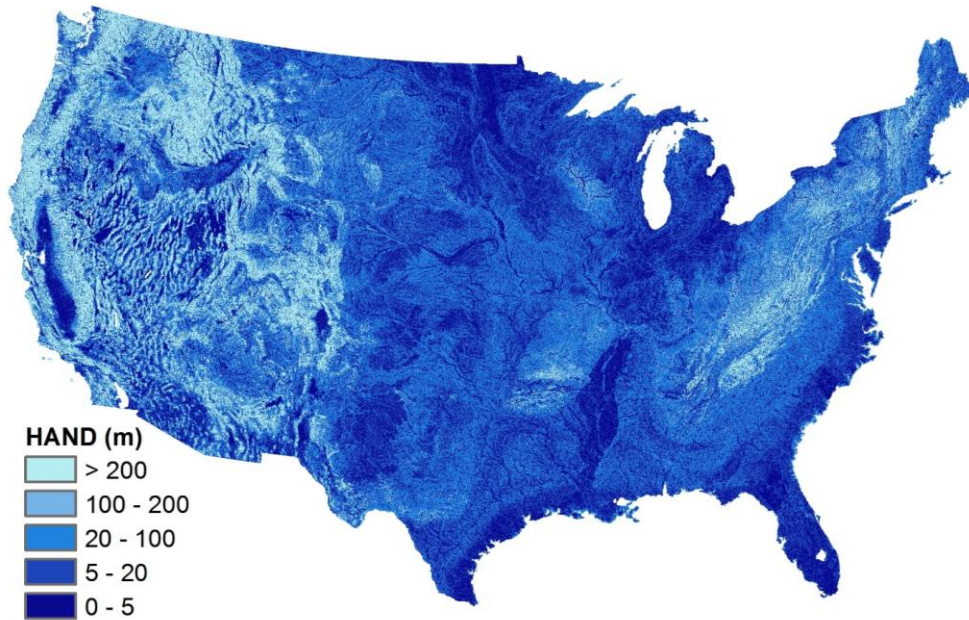
1090

1091 Figure 10. The comparison of the observed saturated area and simulated contributing areas by TOPMODEL and HSC
1092 models.

1093

1094

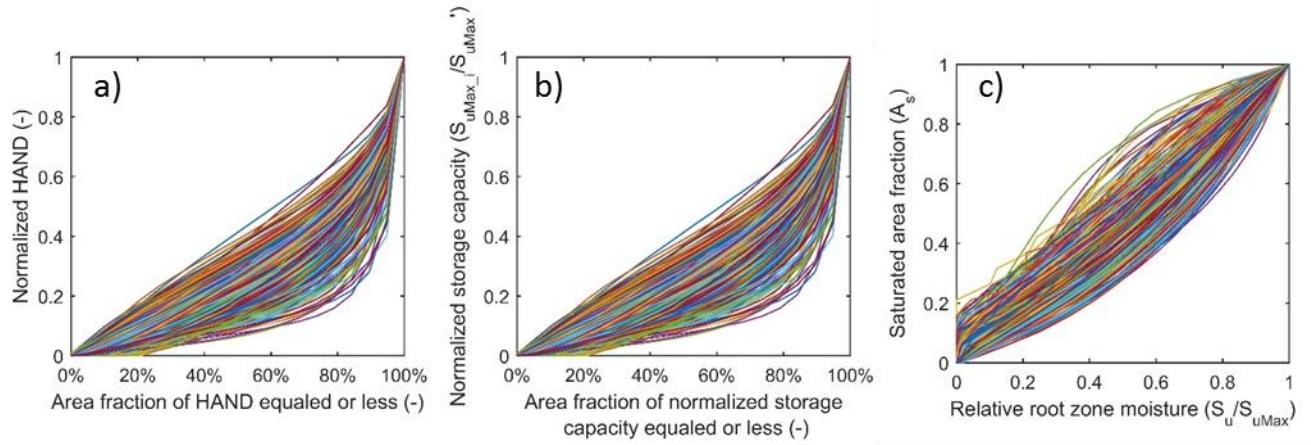
1095



1096

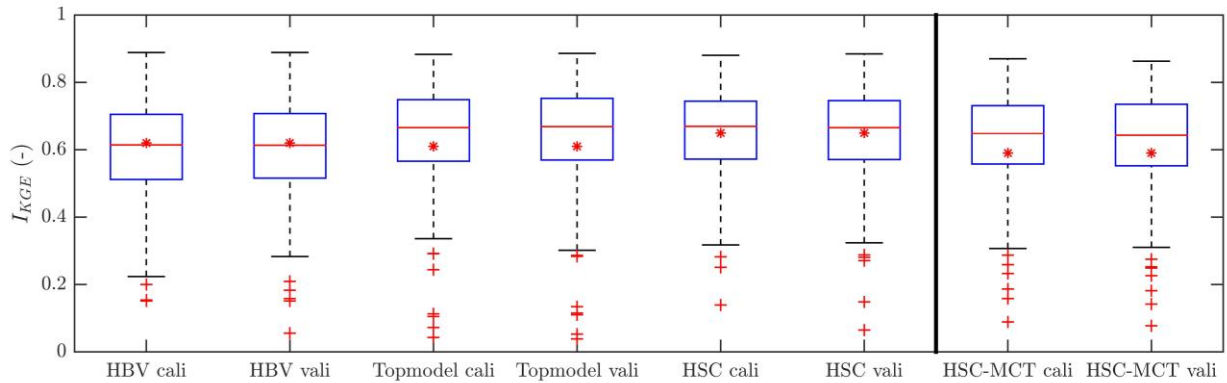
1097 Figure 11. The Height Above the Nearest Drainage (HAND) map of the CONUS.

1098
1099



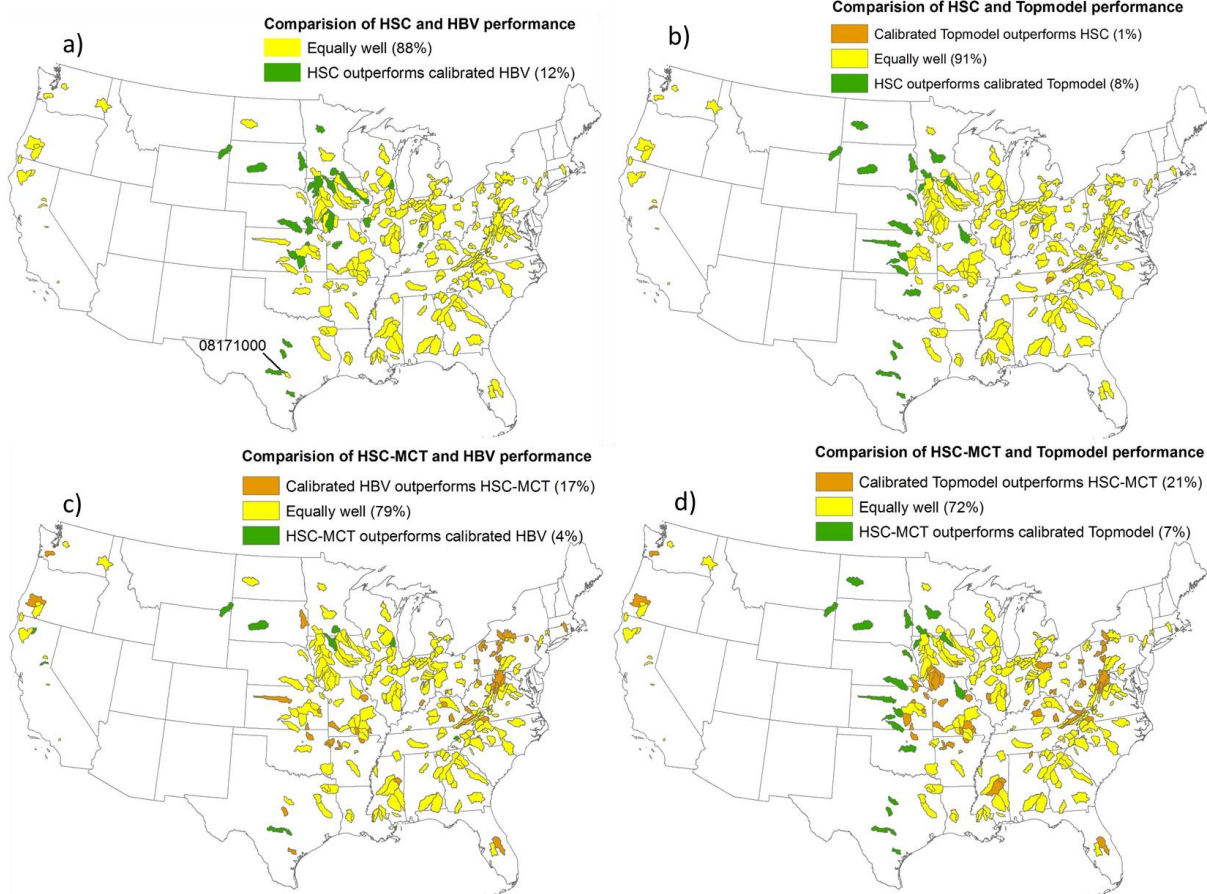
1100
1101
1102
1103
1104

Figure 12. a) The profiles of the normalized HAND of the 323 MOPEX catchments; b) the relations between area fraction and the normalized storage capacity profile of the 323 MOPEX catchments; c) the S_u - A_s curves of the HSC model which can be applied to estimate runoff generation from relative soil moisture for the 323 MOPEX catchment.



1105
1106
1107

Figure 13. The comparison between the HBV, the TOPMODEL, the HSC, and the HSC-MCT models



1108

1109 Figure 14. Performance comparison of the HSC and HSC-MCT models compared to two benchmarks models: HBV

1110 and TOPMODEL, for the 323 MOPEX catchments.